TUM

TECHNISCHE UNIVERSITÄT MÜNCHEN
INSTITUT FÜR INFORMATIK

Path-Wise Algorithms for Random & Stochastic ODEs with Applications to Ground-Motion-Induced Excitations of Multi-Storey Buildings

Tobias Neckel, Alfredo Parra Hinojosa, Florian Rupp

TUM-I1758

Technischer Bericht
Technische Universität München
Institut für Informatik

Path-Wise Algorithms for Random & Stochastic ODEs with Applications to Ground-Motion-Induced Excitations of Multi-Storey Buildings

Tobias Neckel & Alfredo Parra Hinojosa

Chair of Scientific Computing, Technische Universität München, Fakultät für Informatik, D-85747 Garching, Germany

Florian Rupp

Department of Mathematics & Science, German University of Technology in Oman (GUtech), PO Box 1816, Athaibah PC 130, Muscat, Sultanate of Oman

neckel@in.tum.de , hinojosa@in.tum.de , florian.rupp@gutech.edu.om

Abstract

Random effects play a vital role in various physical phenomena and have to be addressed in the mathematical modeling and numerical simulations of such processes. In this contribution, the concepts of random (ordinary) differential equations (RODEs) and stochastic (ordinary) differential equations (SODEs) are reviewed. Details concerning the numerical solution of problems formulated via SODEs and RODEs are summarised. In particular, key features of the averaged Euler and Heun as well as K-RODE Taylor methods for RODEs are compared with numerical methods for SODEs such as the Euler-Maruyama and the Milstein scheme. Finally, the studied RODE and SODE methods are applied to one- and multi-dimensional examples, including the problem of ground-motion-induced excitations of multi-storey buildings subject to the Kanai-Tajimi earthquake model. Being paradigms for additive white noise driven systems, these applications illustrate on the one hand the applicability of the aforementioned numerical methods on an extremely wide class of problems. On the other hand, the coupled oscillator structure of the earthquake induced motion of multi-storey buildings naturally gives rise to the development of hybrid numerical schemes that combine averaged and deterministic schemes to fully exploit their benefits.

keywords: *random differential equation, stochastic differential equation, path-wise solutions, numerical schemes, averaged schemes, Kanai-Tajimi model, earthquake induced excitation of multi-storey buildings*

MSC (2010): *4Fxx, 60H10, 65Cxx, 68Uxx*

I Introduction

Random ordinary differential equations (RODEs) and their numerics lived, up to now, mostly a shadowy existence outshone by the more prominent white noise driven stochastic ordinary differential equations (SODEs) and Itô's calculus, cf. [20], p. 9. Nevertheless, their conceptually easier formalism, their natural modeling capacity of real processes, and their immediate applicability to additive white noise driven systems as well as new algorithms with high convergence rates seem to justify a closer look at random ordinary differential equations.

Motivated by the excellent algorithmic introductions to the numerics of stochastic ordinary differential equations [14, 20, 26] as well as the outstanding works on numerical methods for random differential equations [13, 24], the purpose of this article is four-fold: first, to give a concise one-paper survey of the existing methods, useful for applied mathematicians and computer scientists; second, to compare key features of the corresponding methods for random as well as stochastic differential equations; and third, to apply these methods to a realistic problem and compare the results.

In view of this, we state and compare the averaged Euler and Heun as well as *K*-RODE Taylor methods for random (ordinary) differential equations with the Euler-Maruyama and the Milstein schemes for stochastic (ordinary) differential equations.

These numerical methods are applied to a problem beyond the mathematical toy box of one-dimensionality, namely the ground-motion induced excitation of multi-storey buildings subject to the Kanai-Tajimi earthquake model, cf. [21, 22, 34]. Here, the Doss-Sussmann/ Imkeller-Schmalfuss correspondence, cf. [8, 16, 33], allows us to transform the stochastic differential equation given by this model into its path-wise equivalent random differential equation and apply all above mentioned numerical methods to this case.

Interestingly enough, there are well-established additive white noise models in finance, like the continuous Vasicek model, the extended Vasicek model, the Hull-White model, the Black-Karasinski model or the Black-Derman-Toy model for interest rates, cf. [3], among others, that can be treated the same way and are, thus, accessible for the much easier theory of RODEs and their numerical schemes that have the same order of convergence as expected from corresponding deterministic schemes and have thus a slight advantage over the usual schemes for SODEs, as we will see later.

Our article is structured as follows: In Sec. II, we recall the theory of random and stochastic differential equations together with a small outline of their mathematical foundations as well as the Doss-Sussmann/ Imkeller-Schmalfuss correspondence. Moreover, as a direct application of the Doss-Sussmann/ Imkeller-Schmalfuss correspondence, we introduce a mathematical ansatz for ground-motion induced excitation of multi-storey buildings subject to the Kanai-Tajimi earthquake model.

In Sec. III, explicit numerical schemes for random differential equations are discussed together with their properties of strong convergence. In particular, the averaged Euler and averaged Heun as well as *K*-RODE Taylor methods are studied and applied to the problem of simulating ground-motion-induced excitation of multi-storey buildings. These buildings are modeled in the sense of wire-frame structures that obey damped oscillation equations. In this context, a method common in the engineering literature—called Frequency Response Analysis—is discussed and compared to the convergence results obtained for the averaged Euler scheme. Moreover, the special structure of a ground-motion excited multi-storey building as a system of coupled oscillators allows the discussion of hybrid random/ deterministic methods that compute the ground motion excitation with the aid of the averaged Euler method and then use this for the computation of the movement of the building with the aid of a (deterministic) Euler method. Here, the application of this hybrid

approach works due to the smoothing properties of the Kanai-Tajimi earthquake model.

Section IV briefly covers the corresponding explicit numerical schemes for stochastic differential equations together with their properties of strong convergence. The methods explicitly discussed are just the Euler-Mayurama and the Milstein scheme to have a consistent basis of comparison with the low order RODE methods studied in Sec. III. For higher-order schemes we refer to the literature, in particular to [23] and [26]. We extend our method for the evaluation of multiple Ornstein-Uhlenbeck integrals to the computation of multiple Wiener-integrals. Again, the aforementioned SODE methods are applied to the problem of simulating ground-motion induced excitation of multi-storey buildings and their performance is compared to their RODE counterparts.

Finally, in Sec. V, we give a short summary and outlook on further interesting topics of research that can be founded on this article.

II Random and Stochastic Ordinary Differential Equations and Their Path-Wise Solutions

In order to be self-contained, we start with a short overview of the mathematical foundations before we recall the mathematical theorems that account for path-wise existence and uniqueness of random ordinary differential equations and stochastic ordinary differential equations, further details can be found in [4] and [29]. For fixed realisations of their driving stochastic process, RODEs can be considered as deterministic ordinary differential equations. Nevertheless, due to the nature of the Wiener process, SODEs must be considered in a mean-square sense such that the notion of "path-wise" has, strictly speaking, different interpretations for these two types of differential equations. On the other hand, from a topological point of view, the Doss-Sussmann/ Imkeller-Schmalfuss correspondence establishes a realisation-wise conjugacy between RODEs and SDOEs that will be applied to transfer the famous Kanai-Tajimi earthquake model from an SODE to an RODE and, thus, make it accessible to a comparison for both approaches.

II.1 Mathematical Foundations

Let us first recall the definition of Hölder and Lipschitz continuity as well as that of $C^{k,\alpha}$-functions, cf. for instance [1], p. 40:

Definition 1 (Hölder and Lipschitz Continuity/ $C^{k,\alpha}$-functions)**.** *Let $(X, \|\cdot\|_X)$, $(Y, \|\cdot\|_Y)$ be normed spaces and $0 < \alpha \leq 1$. A function $f : X \to Y$ is called* globally Hölder continuous *of order α if there is a positive constant C such that*

$$\|f(x) - f(y)\|_Y \leq C\|x - y\|_X^\alpha \qquad \forall\, x, y \in X\,. \tag{II.1}$$

f is called locally Hölder continuous *of order α if it satisfies the condition (II.1) on every bounded subset of X. f is called* globally (locally) Lipschitz continuous *if it is globally (locally) Hölder continuous of order $\alpha = 1$. f is called a $C^{k,\alpha}$-function if it is k times continuously differentiable and the k-th derivative is locally Hölder continuous of order α for some $k \in \mathbb{N}$.*

From the illustrative point of view, white noise w_t is a signal (or process), named in analogy to white light, with equal energy over all frequency bands. Mathematically, white noise w_t is characterised by the following properties:

Definition 2. *A* white noise process $(w_t)_{t\in\mathbb{R}_0^+}$ *has vanishing mean, i.e., $\mathbb{E}(w_t) = 0$, and its auto-correlation is δ-distributed, i.e., $\mathbb{E}(w_t w_s) = \delta(t - s)$.*

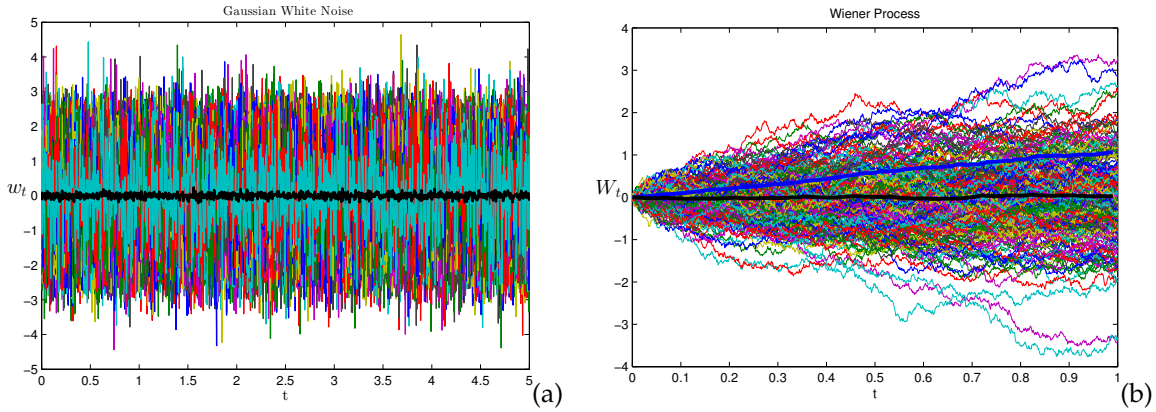

Figure 1: 2 sample paths of the white noise process together with its mean (thin black) (a) and 200 sample paths of the Wiener process together with its mean (thick black) and variance (thick blue) (b).

Formally, the Wiener process W_t is the "integral" of w_t:

$$W_t \;=\; \int_0^t w_s \mathrm{d}s \qquad \text{or} \qquad \mathrm{d}W_t \;=\; w_t \mathrm{d}t\,.$$

Again, we define it properly by its characteristic properties:

Definition 3. *The* Wiener process $(W_t)_{t\in\mathbb{R}_0^+}$ *is characterised by the following three properties:*

1. $W_0 = 0$ *(with probability* 1*),*
2. W_t *has independent increments, i.e., for* $0 = t_0 < t_1 < t_2 < \cdots < t_n < \infty$ *the differences* $W_{t_1} - W_{t_0}$, $W_{t_2} - W_{t_1}, \ldots, W_{t_n} - W_{t_{n-1}}$ *are (mutually) independent, and*
3. *the increments are normally distributed, i.e.,* $W_t - W_s \sim \mathcal{N}(0, t-s)$ *for* $0 \leq s < t$*, where* $\mathcal{N}(0, t-s)$ *denotes the normal distribution with expectation* 0 *and variance* $t - s$*.*

Figure 1 gives some illustrative sample paths of the white noise process and the Wiener process. In particular the properties $\mathbb{E}(w_t)$, $\mathbb{E}(W_t)$ and $\mathbb{V}ar(W_t)$ are clearly visible.

Historically, the Wiener process was the first interpretation of Brown's experiment: in 1827 the Scottish botanist Robert Brown (21.12.1773–10.06.1858) observed that microscopic particles suspended in liquid make very strange and highly irregular movements. Nearly one hundred years later, in 1923 Norbert Wiener (26.11.1894–18.03.1964) gave the first acknowledged and concise definition of a mathematical model for Brown's experiment. For some very nice derivations of the mathematical modeling for the motion of a Brownian particle we refer to [2], p. 101, and [6].

White noise and the Wiener process are examples of stochastic processes.

Definition 4. *Let* $(\Omega, \mathcal{A}, \mathbb{P})$ *be a probability space*[1]*,* $(\mathbb{R}^n, \mathcal{B}(\mathbb{R}^n))$ *the n-dimensional Euclidean space endowed with the Borel-*σ*-algebra, and* $I = [t_0, T] \subseteq \mathbb{R}_0^+$*. At a fixed time* $\tau \in I$*, a random variable* $X_\tau(\omega)$ *of* $\mathbb{R}^n$ *is a map* $X_\tau : \Omega \to \mathbb{R}^n$ *which is* $\mathcal{A} - \mathcal{B}(\mathbb{R}^n)$ *measurable.*

- *A* stochastic process X_t *is a collection* $\{X_\tau(\omega) : \tau \in I\}$ *of random elements in* $\mathbb{R}^n$*.*

[1] I.e., $\mathcal{A}$ is a σ-algebra on the nonempty set Ω, and $\mathbb{P}$ is a probability measure on the measurable space $(\Omega, \mathcal{A})$.

- *For each $\omega \in \Omega$, the map $I \ni t \mapsto X_t(\omega)$ is called a* sample path, trajectory *or* realisation *of X_t.*

Concerning stochastic processes $(X_t)_{t\in\mathbb{R}_0^+}$, we often suppress the notation as a series of time points and only write X_t instead, or $X(t)$ if there is no confusion with deterministic functions.

II.2 Random Ordinary Differential Equations (RODEs)

Our main source for the set-up and discussion of random differential equations will be [4]. We denote by S_d the set of all d-dimensional random-vectors. Let $X : I \times \Omega \to \mathbb{R}^m$ be an $\mathbb{R}^m$-valued stochastic process with continuous sample paths, and $f : \mathbb{R}^d \times I \times \Omega \to \mathbb{R}^d$ be a continuous function.

Definition 5. *A* random (ordinary) differential equation *(short: random differential equation) on $\mathbb{R}^d$,*

$$\frac{\mathrm{d}X_t}{\mathrm{d}t} \;=\; f(X_t(\cdot), t, \omega)\,, \qquad X_t(\cdot) \in \mathbb{R}^d\,, \tag{II.2}$$

is a non-autonomous ordinary differential equation

$$\dot{x} \;=\; \frac{\mathrm{d}x}{\mathrm{d}t} \;=\; F_\omega(x,t)\,, \qquad x \;:=\; X_t(\omega) \in \mathbb{R}^d \tag{II.3}$$

for almost all $\omega \in \Omega$. Again, for notational simplicity, we often suppress the argument ω if no ambiguities result.

A stochastic process X_t defined on the interval I is called path-wise solution *of the random differential equation (II.2) if almost all realisations of X_t on I are solutions of the non-autonomous deterministic ordinary differential equation (II.3).*

Let $t_0 \in I$ and let $X_0 \in S_d$ such that $X_{t_0} \hat{=} X_0$. Then, X_t is called path-wise solution of (II.2) with respect to the initial condition (X_0, t_0).

The path-wise solution of (II.2) with respect to the initial condition (X_0, t_0) is called unique *on I if for an arbitrary pair X_t and X_t^* of path-wise solutions with respect to the initial condition (X_0, t_0) the following holds true:*

$$X_t \;\overset{I}{=}\; X_t^*\,.$$

Reformulating this definition, we have that we associate a deterministic (ordinary) differential equation to any realisation $\omega \in \Omega$. The solutions of these deterministic differential equations are the realisations of a stochastic process, which is the path-wise solution of the random differential equation (II.2).

Thus, in order to show the existence of path-wise solutions one first plays this issue back to the theory of deterministic (ordinary) differential equations and shows that (II.3) has a solution on an ω-independent interval $I \subset \mathbb{R}_0^+$ for almost all $\omega \in \Omega$.

Theorem 1. *Let the following three prerequisites be satisfied:*

1. *The functions $f(x,t,\omega)$ are $\mathcal{A}$-measurable for all $(x,t) \in \mathbb{R}^d \times I$.*
2. *$f(x,t,\omega)$ is continuous on $\mathbb{R}^d \times I$ for almost all $\omega \in \Omega$.*
3. *For almost all $\omega \in \Omega$ there is a real continuous function $L(t,\omega)$ on I such that*

$$\|f(x_1,t,\omega) - f(x_2,t,\omega)\| \;\leq\; L(t,\omega)\|x_1 - x_2\|\,,$$

where $t \in I$ and $x_1, x_2 \in \mathbb{R}^d$.

Then, for any initial condition $(X_0, t_0) \in S_d$ there exists a unique path-wise solution on I of the random differential equation (II.2).

Proof. The proof is given in [4], Theorem 1.4, p. 18. □

Next, we state the technically more advanced concept of white-noise-driven stochastic differential equations.

II.3 Stochastic Ordinary Differential Equations (SODEs)

Combining a deterministic part (the drift) and a white-noise driven part (the diffusion) leads to a stochastic differential equation:

$$\mathrm{d}X_t \;=\; \underbrace{a(X_t,t)}_{\text{drift}}\,\mathrm{d}t \;+\; \underbrace{b(X_t,t)}_{\text{diffusion}}\,\mathrm{d}W_t\,.$$

As for ordinary differential equations, this notation is equivalent to the integral representation of the solution process X_t

$$X_t \;=\; X_0 \;+\; \int_{t_0}^{t} a(X_s,s)\mathrm{d}s \;+\; \int_{t_0}^{t} b(X_s,s)\mathrm{d}W_s \tag{II.4}$$

with initial value $X_{t_0} = X_0$ at the initial time t_0, where the identity holds almost surely. The first integral on the right hand side of (II.4) is well defined as a usual Riemann or Lebesgue integral, whereas the integral with respect to the Wiener process has to be properly interpreted[2]. This was first achieved by Kiyoshi Itô (07.09.1915–10.11.2008).

In the case of ordinary differential equations, the simplest existence and uniqueness theorem assumes that the right-hand-side coefficient function $a(x,t)$ satisfies a Lipschitz condition in x and is bounded with respect to t for some x (growth condition). Similar restrictions on the drift and diffusion part ensure the existence and uniqueness of the solution of a stochastic differential equation:

Theorem 2. *Let $a(x,t) = (a_1(x,t),\ldots,a_n(x,t))^T$, $B(x,t) = (B_{ij}(x,t))_{i,j=1,\ldots,n}$ be measurable on $\mathbb{R}^n \times [0,T]$ and satisfy the uniform Lipschitz-condition*

$$|a(x_1,t) - a(x_2,t)| \;\leq\; K_*|x_1 - x_2|\,, \qquad |B(x_1,t) - B(x_2,t)| \;\leq\; K_*|x_1 - x_2|$$

and the growth restriction

$$|a(x,t)| \;\leq\; K(1+|x|)\,, \qquad |B(x,t)| \;\leq\; K(1+|x|)\,,$$

for all $x, x_1, x_2 \in \mathbb{R}^n$, $t \in [0,T]$, with positive constants K_*, K. Let X_0 be constant. Then there exists a path-wise unique solution of

$$\mathrm{d}X_t = a(X_t,t)\mathrm{d}t \;+\; B(X_t,t)\underline{\mathrm{d}W_t}\,, \tag{II.5}$$

$$X(0) = X_0\,, \tag{II.6}$$

on the space-time cylinder $(x,t) \in \mathbb{R}^n \times [0,T]$, where $\underline{W_t}$ denotes the n-dimensional Wiener process.

[2] Riemann(-Stieltjes) integrals $\int_{t_0}^{t} f(s)\mathrm{d}g(s)$ of a function f against another function g are defined only for functions g with bounded variation, see the Theorem of Banach-Steinhaus (cf. [31]). Unfortunately, the Wiener process is of unbounded variation.

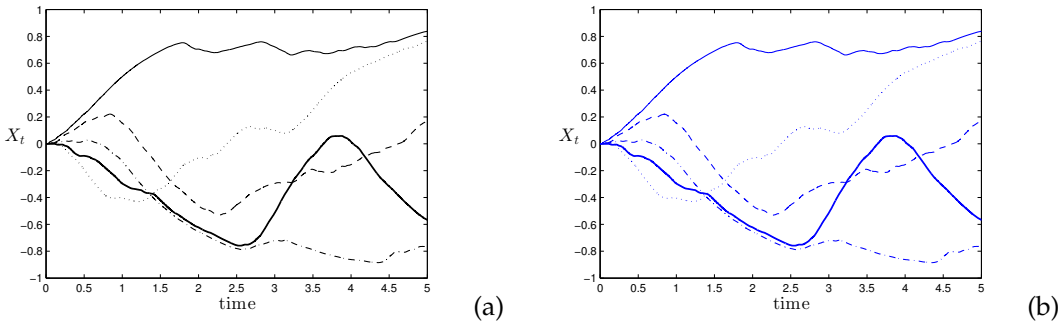

Figure 2: Five sample paths of $\dot{X}_t = -X_t + \sin(W_t(\omega))$ computed by the the averaged Euler schema for RODEs with step size $1/1024$ (a) and the corresponding SODE computed by stochastic Euler-Mayurama schema (b). The results are indistinguishable up to truncation precision.

Proof. The proof is given in [9], pp. 98. □

For stochastic differential equations, the notion of *path-wise uniqueness* means that if $X_1(t)$ and $X_2(t)$ are two solutions of (II.5), (II.6), then

$$\mathbb{P}\left(X_1(t) = X_2(t) \text{ for all } t \in [0,T]\right) \;=\; 1\,,$$

i.e., there may only be a subset $\tilde{\Omega} \subset \Omega$ of vanishing measure such that $X_1(\tilde{t})(\tilde{\omega}) \neq X_2(\tilde{t})(\tilde{\omega})$ for $\tilde{\omega} \in \tilde{\Omega}$ at a time $\tilde{t} \in [0,T]$.

II.4 The Doss-Sussmann/ Imkeller-Schmalfuss Correspondence

Random differential equations with Wiener processes can be re-written as stochastic differential equations, so that results for the one type of equations can be applied to the other and vice versa, cf. [20], pp. 10.

Example 1. *(From an RODE to an SODE, cf. [20], p. 10.) The scalar random differential equation $\dot{X}_t = -X_t + \sin(W_t(\omega))$ can be re-written as the following two-dimensional stochastic differential equation*

$$\mathrm{d}\begin{pmatrix} X_t \\ Y_t \end{pmatrix} \;=\; \begin{pmatrix} -X_t + \sin(Y_t) \\ 0 \end{pmatrix} \mathrm{d}t \;+\; \begin{pmatrix} 0 \\ 1 \end{pmatrix} \mathrm{d}W_t\,.$$

Figure 2 displays sample paths of this equation that are computed via the averaged Euler scheme for random ordinary differential equations 2(a) and via the stochastic Euler-Mayurama scheme for stochastic ordinary differential equations 2(b).

Following [20], pp. 10, we observe that any (finite-dimensional) stochastic differential equation can be transformed to a random differential equation: In the case of commutative noise, this is a famous result obtained by Halim Doss and Hector J. Sussmann (see [8], [33]), which was generalised in 1998 to all stochastic differential equations by Peter Imkeller and Björn Schmallfuss (cf. [16]). This *Doss/ Sussmann & Imkeller/ Schmalfuss correspondence* is easily illustrated for a scalar stochastic differential equation with additive noise.

Example 2. *(From a SODE to a RODE, cf. [20], pp. 10.) The scalar stochastic differential equation*

$$\mathrm{d}X_t \;=\; f(X_t)\mathrm{d}t \;+\; \mathrm{d}W_t$$

is equivalent to the random differential equation

$$\dot{Z}_t \;=\; f(Z_t + O_t) + O_t\,,$$

where $Z_t := X_t - O_t$ *and* O_t *is the stationary* Ornstein-Uhlenbeck process *satisfying the stochastic differential equation* $\mathrm{d}O_t = -O_t\mathrm{d}t + \mathrm{d}W_t$*. Note, the Ornstein-Uhlenbeck process is a Gaussian process, and thus it is already uniquely determined by its first two moments.*

Important and meaningful examples of well-recognised models where this correspondence can be applied are the continuous Vasicek model, the extended Vasicek model, the Hull-White model, the Black-Karasinski model, or the Black-Derman-Toy model for short-term interest rates (cf. [3]), or the Kanai-Tajimi model for earthquake-induced ground motion excitations.

II.5 Simulating Ground-Motion-Induced Excitation of Multi-Storey Buildings

Kanai [21], [22] and Tajimi [34] introduced a now commonly used model for earthquake induced ground excitations which is based on the following observations, see [28], pp. 78.

> For most earthquake engineering purposes, the earth can be considered as a stratified half-plane, with generally lighter material in an upper layer than the one below. If the source of an earthquake is reasonable deep, then as seismic waves propagate to the ground surface, their direction of propagation is almost vertically upward, as can be explained by Snell's law of refraction. As a first approximation, we may take into account only the uppermost layer between the ground surface and the nearest bedrock and treat the wave propagation in this layer as being one-dimensional and vertical. In the Kanai-Tajimi model, this layer is further approximated by a single-degree of freedom linear system, [28], p. 80.

The Kanai-Tajimi model displays the characteristic properties of real earthquakes for high frequencies quite well, despite its inaccuracies at low frequencies as [30], pp. 19, points out. To improve the Kanai-Tajimi model with respect to a better resolution of the low frequencies, Clough and Penzien suggested in [7] to take the Kanai-Tajimi response as the input of a second linear filter. Both, the Kanai-Tajimi model and the Clough-Penzien model lead to quasi-stationary ground motion excitations, whereas real earthquakes are reported to be non-stationary. In more advanced seismic discussions, envelope functions are combined with stationary models or non-stationarity is introduced by time-dependent additional functions in the Kanai-Tajimi or the Clough-Penzien model, cf. [18, 28, 32, 35]. Since the Kanai-Tajimi model represents a relatively simple but still decently sophisticated approach to realistic stochastic excitations and propagations for our purpose of applying different numerical schemes, we use it in this contribution and summarise its notation in the following paragraph.

Following [30], pp. 18, the stochastic differential equation formulation for the ground motion excitation $\ddot{u}_g(t)$ in the sense of the Kanai-Tajimi model is given as

$$\ddot{u}_g \;=\; \ddot{x}_g + \xi_t \;=\; -2\zeta_g\omega_g\dot{x}_g - \omega_g^2 x_g\,,$$

where x_g is the solution of a zero-mean Gaussian white noise ξ_t driven stochastic oscillator

$$\ddot{x}_g + 2\zeta_g\omega_g\dot{x}_g + \omega_g^2 x_g \;=\; -\xi_t\,, \qquad x_g(0) = \dot{x}_g(0) = 0\,. \tag{II.7}$$

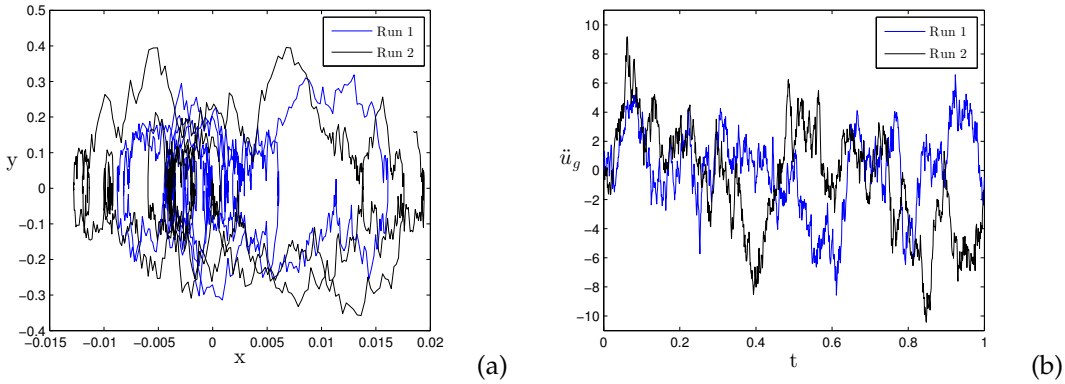

Figure 3: In (a) 2 simulation runs of the SDE Kanai-Tajimi model are displayed in the x-y-plane with initial condition $(x_0, y_0) = (0, 0)$. These are taken to display the acceleration $\ddot{u}_g(t)$ over the time axis in (b).

Here, ζ_g and ω_g are model parameters reflecting the local geological site conditions. For instance, in [15] the use of $\zeta_g = 0.64$ and $\omega_g = 15.56\,[rad/sec]$ is recommended for firm soil conditions in a frequency range from $f = 2.1\,[rad/sec]$ to $f = 21\,[rad/sec]$.

Applying the Doss-Sussmann/ Imkeller-Schmalfuss correspondence allows us to transform the stochastic differential equation (II.7), written as a first-order system,

$$\mathrm{d}\begin{pmatrix} x \\ y \end{pmatrix} = \begin{pmatrix} -y \\ -2\zeta_g\omega_g y + \omega_g^2 x \end{pmatrix}\mathrm{d}t + \begin{pmatrix} 0 \\ 1 \end{pmatrix}\mathrm{d}W_t\,,$$

into the path-wise equivalent random differential equation

$$\begin{pmatrix} \dot{z}_1 \\ \dot{z}_2 \end{pmatrix} = \begin{pmatrix} -(z_2 + O_t) \\ -2\zeta_g\omega_g(z_2 + O_t) + \omega_g^2 z_1 + O_t \end{pmatrix}, \tag{II.8}$$

where O_t is the usual Ornstein-Uhlenbeck process.

Figure 3 shows sample paths of the Kanai-Tajimi model and the excitations they induce on the Earth's surface.

II.6 The Wire-Frame Model of a Multi-Storey Building

In the spirit of [5], pp. 50, the forces acting on the mass on top of the weightless frame of a building are the *external force* $p(t)$ as well as the *damping* resisting force $f_D(t)$ and the *elastic* (or *inelastic/ rigid*) resisting force $f_S(t)$ of the structure.

The external force p is taken to be positive in the direction of the x-axis. The displacement $u(t)$, the velocity $\dot{u}(t)$ and the acceleration $\ddot{u}(t)$ are also positive in the direction of the x-axis. The damping (f_D) and elastic/inelastic (f_S) forces are acting in the opposite direction because they are internal forces and resist the velocity and deformation respectively.

The resultant force along the x-axis is $p - f_D - f_S$ and, finally, Newton's second law of motion gives

$$p - f_S - f_D = m\ddot{u} \qquad \text{or} \qquad m\ddot{u} + f_D + f_S = p\,. \tag{II.9}$$

Now, we require to obtain the resisting forces f_D and f_S. In the case of a d-storey building ($d = 1, 2, \ldots$), the forces F_j that act on a floor j can be split into those resulting from a component

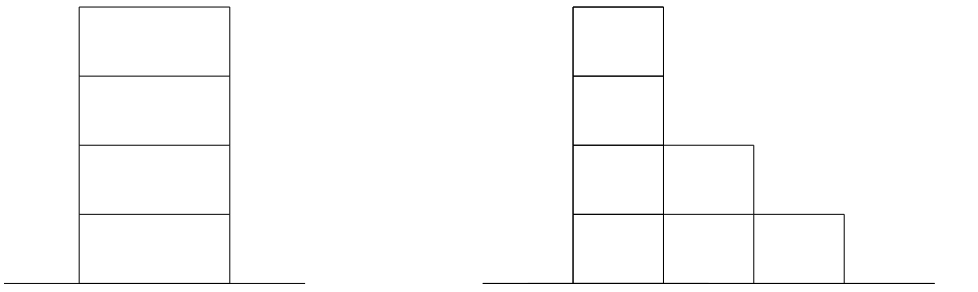

Figure 4: Sketches of the building types we are considering: (a) "normal" 4-storey building and (b) "L-shaped" 4-storey building.

that belongs to the floor above (F_j^{j+1}) and one that belongs to the floor below it (F_j^{j-1}), i.e.,

$$F_j \;=\; F_j^{j-1} \,+\, F_j^{j+1}\,,$$

where we set $F_d^{d+1} = 0$, since there is no external force acting on the roof, and F_1^0 equal to the forces induced by the earthquake. This leads to the following form of the deformation and damping forces where displacements are measured relative to the j-th floor: With some material dependent positive real constants k_j and k_{j+1} as well as c_j and c_{j+1}, the deformation force reads

$$f_S^{(j)} \;=\; k_j\left(u_j - u_{j-1}\right) + k_{j+1}\left(u_j - u_{j+1}\right) \;=\; -k_j u_{j-1} + (k_j + k_{j+1})u_j - k_{j+1}u_{j+1}\,,$$

and the damping force is

$$f_D^{(j)} \;=\; c_j\left(\dot{u}_j - \dot{u}_{j-1}\right) + c_{j+1}\left(\dot{u}_j - \dot{u}_{j+1}\right) \;=\; -c_j\dot{u}_{j-1} + (c_j + c_{j+1})\dot{u}_j - c_{j+1}\dot{u}_{j+1}\,.$$

For $u := (u_1, u_2, \ldots, u_d)^T$, the dimension-free equation of motion in matrix-vector notation has the form

$$\ddot{u} \,+\, C\dot{u} \,+\, Ku \;=\; F(t)\,, \tag{II.10}$$

with a time-dependent external force F corresponding to the earthquake excitation. The matrix K has the structure

$$K \;=\; \begin{pmatrix} k_1 + k_2 & -k_2 & & & \\ -k_2 & k_2 + k_3 & -k_3 & & \\ & -k_3 & k_3 + k_4 & -k_4 & \\ & & \ddots & & \\ & & & -k_d & +k_d \end{pmatrix}$$

and C is analogous. If required, masses are included into the model via diagonal matrices.

For illustration purposes, we apply the numerical schemes for RODEs and SODEs we are about to discuss on two types of buildings as sketched in Fig. 4: a "normal" 4-storey building and an "L-shaped" 4-storey building. Both of these structures will be considered subject to the excitation induced by the Kanai-Tajimi model.

After this theoretical background, we are now going to describe the various numerical algorithms, starting with explicit numerical schemes for random differential equations.

III Explicit Numerical Schemes for Random Differential Equations

Following [13], we assume that the function f in (II.2) is infinitely often continuously differentiable in X_t and ω, but the resulting right-hand side $F_\omega(x,t)$ is usually only continuous (at most Hölder continuous) and not differentiable in t [13, 24, 20]. This point can be illustrated with the use of the previous Example 1. Consider the RODE given by

$$\dot{X}_t = -X_t + \sin(W_t(\omega)), \tag{III.1}$$

where $W_t(\omega)$ is a sample path of a Wiener process. It is known from the theory of RODEs [4] that the solution of (III.1) is given by

$$X_t = e^{-t}X_0 + e^{-t}\int_{t_0}^{t} e^{\tau}\sin\left(W_\tau(\omega)\right)\mathrm{d}\tau. \tag{III.2}$$

The sample paths of $W_t(\omega)$ are Hölder continuous but nowhere differentiable, so the solution X_t is only once differentiable. This property directly affects the order of convergence of the standard numerical schemes (e.g. Euler, Heun, Runge-Kutta), since the Taylor expansions needed for their error analyses cannot be carried out. Let us turn our attention to this fact, which is presented in detail in [13].

Consider the class of explicit one-step numerical schemes for Eq. (II.2) given by

$$x_{n+1} = x_n + h_n\phi(h_n, t_n, x_n), \tag{III.3}$$

at discretised timesteps $t_n \in [t_0, T]$ and step sizes $h_n = t_{n+1} - t_n \in (0, h]$ for all $n = 0, ..., N-1$. In particular, for a fixed ω, let $F_\omega(x,t) := f(x,t)$ in Eq. (II.2), where f is assumed to be locally Lipschitz continuous in x (with $|x(t)| \leq R$, $R(w) = R > 0$, for all $t \in [t_0, T]$) with Lipschitz constant L_R. Denote $B[0;R] := \{x \in \mathbb{R}^d : |x| \leq R\}$. Furthermore, let $M_R = \max_{t\in[0,T], x\in B[0;R]} |f(x,t)|$. The discretisation error of the schemes (III.3) will be given in terms of the moduli of continuity of f and ϕ, defined as

$$\omega_f(h) := \omega_f(h;R,T) = \sup_{\substack{s,t\in[0,T]\\ 0\leq|s-t|\leq h}} \sup_{x\in B[0;R]} |f(t,x) - f(s,x)|, \tag{III.4a}$$

$$\omega_\phi(h) := \omega_\phi(h;R,T) = \sup_{0\leq h_n\leq h} \sup_{\substack{t\in[0,T]\\ x\in B[0;R]}} |\phi(h_n,t,x) - \phi(0,t,x)|. \tag{III.4b}$$

Under these considerations, the following theorem holds.

Theorem 3. *The global discretisation error of the numerical scheme III.3 satisfies the estimate*

$$|x_n - x(t_n;t_0,x_0)| \;\leq\; \frac{\omega_f(h) + \omega_\phi(h) + L_R M_R h}{L_R}\cdot e^{L_R T}. \tag{III.5}$$

Proof. The proof is given in [13]. □

III.1 The Euler & Heun Schemes for RODEs

The simplest scheme is obtained by taking $\phi(h,t,x) = f(t,x)$, where (III.4b) gives $\omega_\phi(h) = 0$. The global discretisation error of this explicit Euler scheme is then given by

$$|x_n - x(t_n;t_0,x_0)| \;\leq\; \frac{\omega_f(h) + L_R M_R h}{L_R}\cdot e^{L_R T} \;=\; O(\omega_f(h)), \tag{III.6}$$

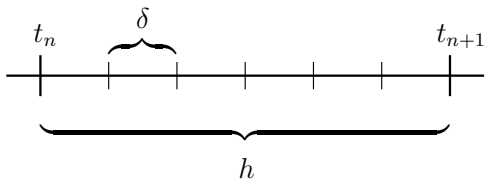

Figure 5: Visualisation of the subcycling for the averaging: in each time step of step size h, a further subdivision using a (considerably) smaller step size $\delta = h/N$ has to be used.

the last step following from the Hölder continuity of f in t, Eq. (II.1). This result is to be compared with the usual error estimate of Euler's method for ODEs, which is of order h (cf. [12]). The error estimate reflects the close relation between the order of the scheme and the order of the Hölder continuity of f. Such result is illustrated in [20] for the RODE

$$\frac{\mathrm{d}x}{\mathrm{d}t} = -x + \zeta_t,$$

where ζ_t is a stochastic process, path-wise Hölder continuous of order $\frac{1}{2}$. The Euler scheme in this case is of path-wise order $\frac{1}{2}$.

The authors in [13] have shown how to attain the upper bound $|x_n - x(t_n; t_0, x_0)| = O(h)$ for a family of RODEs with separable vector field, namely

$$\frac{\mathrm{d}x}{\mathrm{d}t} = G(t) + g(t)H(x), \tag{III.7}$$

where $g : [0,T] \to \mathbb{R}$ has modulus of continuity $\omega_g(\delta)$ on $[0,T]$, $G : [0,T] \to \mathbb{R}^d$ has modulus of continuity $\omega_G(\delta)$ on $[0,T]$, and $H : \mathbb{R}^d \to \mathbb{R}^d$ is at least once continuously differentiable. The method is called *averaged Euler scheme*, since the underlying idea is to substitute the function g by its average

$$\bar{g}^{(1)}_{h,\delta}(t) = \frac{1}{N}\sum_{j=0}^{N-1} g(t + j\delta), \tag{III.8}$$

at every interval $[t, t+h]$ with a sampling step size $\delta = h/N$ (see Fig. 5).

Carrying out the same averaging procedure for the function $G(t)$, one can rewrite (III.3) as

$$\begin{aligned} x_{n+1} &= \frac{1}{N}\sum_{j=0}^{N-1}\{x_n + hG(t_n + j\delta) + hg(t_n + j\delta)H(x_n)\} \\ &= x_n + \frac{1}{N}\sum_{j=0}^{N-1} hG(t_n + j\delta) + \frac{H(x_n)}{N}\sum_{j=0}^{N-1} hg(t_n + j\delta)\ . \end{aligned} \tag{III.9}$$

This averaged Euler scheme has a *local* discretisation error $L(h; x, t)$ given by

$$L(h; x, t) = O(h(\omega_g(\delta) + \omega_G(\delta))),$$

which will be of order 2 if δ is chosen in such a way that $\max\{\omega_g(\delta), \omega_G(\delta)\} = O(h)$, thus attaining a global error of order 1.

The Heun scheme is obtained in an analogous way, this time by defining

$$\phi(h, t, x) = \frac{1}{2}\{f(x,t) + f(t + h, x + hf(x,t))\}.$$

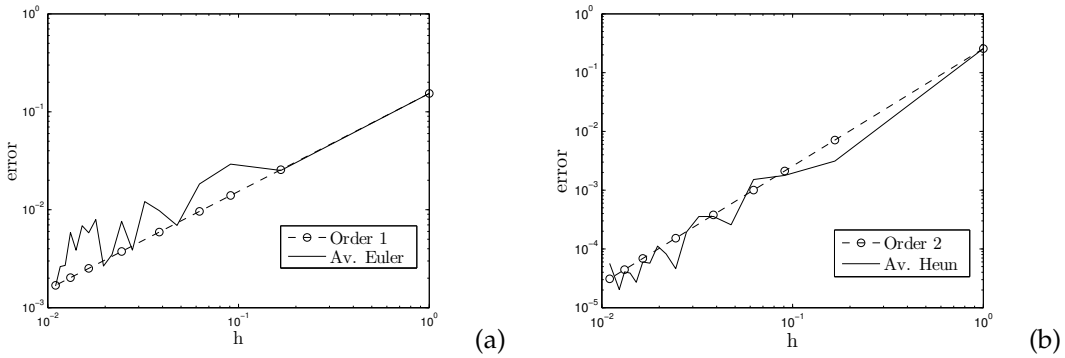

Figure 6: Convergence plots for the averaged Euler scheme (a) and the averaged Heun scheme (b) applied to $\dot{X}_t = -X_t + \sin(W_t(\omega))$ (i.e. Eq. (III.1)). The order of strong convergence 1 for the averaged Euler scheme and of order 2 for the averaged Heun scheme are clearly visible.

Since the modulus of continuity $\omega_\phi(h)$ satisfies $\omega_\phi(h) \leq K_1\omega_f(h)$ for some constant K_1 depending on T and R, the estimate (III.6) for the global discretisation error still holds.

The *averaged Heun scheme* for RODEs with separable right-hand side f follows the same reasoning as above, but the function H is required to be two times continuously differentiable. We now need the double-averaged function

$$\bar{g}^{(2)}_{h,\delta}(t) = \frac{2}{N^2}\sum_{i=0}^{N-1}\sum_{j=0}^{i} g(t+j\delta) = \frac{2}{N^2}\sum_{j=0}^{N-1}(N-j)g(t+j\delta), \tag{III.10}$$

in addition to the single-averaged function above. The resulting scheme is:

$$\begin{aligned} x_{n+1} = x_n &+ h\bar{G}^{(1)}_{h,\delta}(t_n) + \frac{h}{2}\bar{g}^{(1)}_{h,\delta}(t_n)H(x_n) \\ &+ \frac{h}{2}\bar{g}^{(1)}_{h,\delta}(t_n)H\left(x_n + h\bar{G}^{(2)}_{h,\delta}(t_n) + h\bar{g}^{(2)}_{h,\delta}(t_n)H(x_n)\right). \end{aligned} \tag{III.11}$$

The expression for the local discretisation error for the scheme (III.11) is given by

$$L(h;x,t) = O((h+h^2)(\omega_g(\delta) + \omega_G(\delta)) + h^3),$$

which will be of order 3 if δ is chosen such that $\max\{\omega_g(\delta), \omega_G(\delta)\} = O(h^2)$. This ensures the order 2 of the global discretisation error of the averaged Heun scheme.

Analogously to the illustration of the strong order of convergence 1 for the averaged Euler scheme, Figure 6 (b) displays the convergence properties of the averaged Heun scheme applied to Eq. (III.1). Since the Wiener process is Hölder continuous of exponent $1/2$, we obtain $\omega_G(h) = O(h^{1/2})$ so $\delta = h^2$ for the averaged Euler scheme and $\delta = h^4$ for the averaged Heun scheme. This aspect is discussed in more detail in Sec. III.5.

Figure 6 (a) displays the convergence properties of the averaged Euler scheme applied to Eq. (III.1).

III.2 Numerical Results 1: Averaged Euler & Heun Schemes

As said, our aim is to study the performance of RODEs and SODEs for a ground motion excitation of multi-storey buildings via the Kanai-Tajimi earthquake model.

The system of equations for the Kanai-Tajimi model (II.8) has a separable right hand side $f(z,t) = G(t) + g(t)H(z)$, where $z = (z_1, z_2) \in \mathbb{R}^2$, with

$$G(t) = -O_t \begin{pmatrix} 1 \\ 2\zeta_g\omega_g - 1 \end{pmatrix}, \quad H(z) = -\begin{pmatrix} z_2 \\ 2\zeta_g\omega_g z_2 - \omega_g^2 z_1 \end{pmatrix}, \quad g(t) = 1\,. \tag{III.12}$$

Therefore, an implementation of the Averaged Euler and Heun schemes is straightforward, once a realisation of O_t is given. To this end, recall that the Ornstein-Uhlenbeck process satisfies $\mathrm{d}O_t = -O_t\mathrm{d}t + \mathrm{d}W_t$, whose solution is given in explicit form as

$$O_{t+\Delta t} = \mu O_t + \sigma_X n_1, \tag{III.13}$$

where $\mu := e^{-\Delta t}$, $\sigma_X^2 := (1-\mu^2)/2$, and n_1 denotes a sample value of a normally distributed random variable $\mathcal{N}(0,1)$, cf. [10]. In this way, Eq. (III.13) allows us to generate sample paths for O_t. From the relation between the Ornstein-Uhlenbeck process and the Wiener process, we conclude, as previously, that $\omega_G(h) = O(h^{1/2})$, hence the sampling step size is $\delta = h^2$ for the averaged Euler scheme and $\delta = h^4$ for the averaged Heun scheme in order to keep the full order of the corresponding methods.

The linear rate of convergence of the Averaged Euler scheme applied to the Kanai-Tajimi model is shown in Fig. **??** (a). In the engineering sciences such oscillation models are often simulated by transferring the problem into the frequency domain. Let D_0 denote the amplitude of the (Gaussian) white noise ξ_t, $\hat{x}_t$ denoting the Fourier Transform of a stochastic process x_t. The application of the Fourier Transform (FT) on a second order differential equation with constant coefficients $c, d \in \mathbb{R}$ forced by white noise (like the Kanai-Tajimi model) leads to

$$\ddot{x}_t + c\dot{x}_t + dx_t \;=\; \xi_t \quad \xrightarrow{FT} \quad -\omega^2\hat{x}_t + ci\omega\hat{x}_t + d\hat{x}_t \;=\; D_0$$

and thus to

$$\hat{x}_t \;=\; \frac{D_0}{-\omega^2 + ci\omega + d}\,.$$

The Inverse Fourier Transforms results in the solution process x_t. In Fig. **??** (b) the rate of convergence for this approach is plotted for decreasing time step sizes in the simulation of one driving white noise ξ_t. Compared to the application of the averaged Euler scheme, this method has a worse order of convergence of 0.5 as one would expect when dealing with stochastic differential equations driven by white noise. On the other hand, due to the huge amount of analytic machinery utilized, the Fourier method leads to a lower absolute error in this case.

This method is easily extended to coupled oscillator systems like our wire-frame buildings. As said, this procedure is well-known in the engineering sciences and called "Frequency Response Analysis", cf. [5], pp. 851.

Instead of deepening this established method and providing a larger example, we focus on RODE methods to simulate the effects on mechanical wire-frame structures. At this stage, we could either perform a complete computation of the multi-storey building subject to the Kanai-Tajimi excitation with the averaged Euler or Heun schemes as just discussed, or aim for a less expensive alternative: We can argue that the excitation

$$\ddot{u}_g \;=\; -2\zeta_g\omega_g z_2 - \omega_g^2 z_1\,,$$

that drives the deterministic dynamics of the multi-storey building, is the sum of two functions. These functions are the path-wise unique solution of

$$\dot{z} \;=\; G(t) + H(z)\,, \quad z \;=\; (z_1, z_2)^T\,,$$

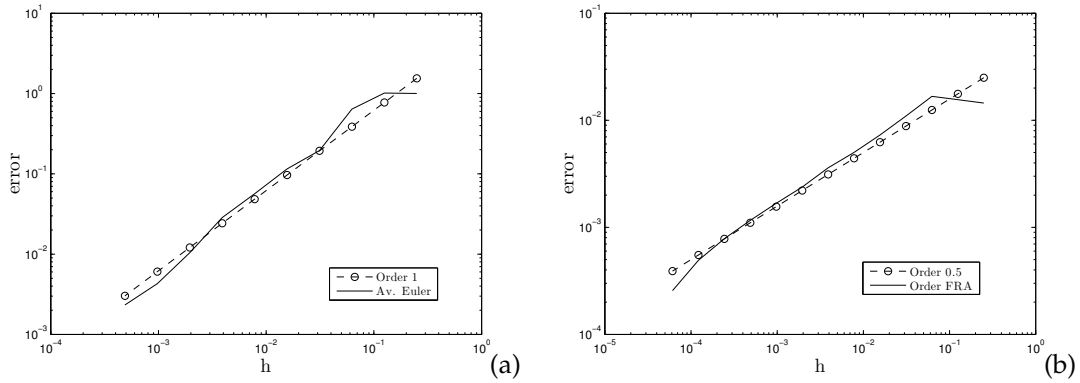

Figure 7: Convergence plots for the averaged Euler scheme (a) and the Freequency Response Analysis (b) applied to the Kanai-Tajimi model.

as stated in Eq. (III.12) with a continuous right hand side. Thus, for any realisation of the underlying continuous random driving process as computed in Eq. (III.13), z_1 and z_2 are continuously differentiable. Hence, from the numerics point of view, we indeed apply a $\mathcal{C}^1$-function $\ddot{u}$ as excitation for our multi-storey buildings. This justifies the use of (low-order) deterministic methods for the final simulation aspects.

In particular, these observations naturally lead to a hybrid scheme consisting of the combination of averaged schemes for the computation of the first transmissions of the stochastic effects through the Kanai-Tajimi model and deterministic schemes for the computation of the oscillations that occur in the single storeys of the building.

Fig. **??** shows one simulation run of different 4-storey buildings under stochastic ground-motion excitation, i.e., Eq. (II.10) with a right-hand side given by the solution of the Kanai-Tajimi model $\ddot{u}_g$ with parameters $\zeta_g = 0.64$ and $\omega_g = 15.56\,[rad/sec]$. (From a geological point of view, these parameters model firm soil conditions.) The Kanai-Tajimi equation is solved with the Averaged Euler scheme using $h = 1/1024$, and the system of equations (II.10) is solved using a deterministic Euler scheme. There, the movement of four different 4-storey buildings under the same stochastic excitation at times a) $t = 0.5$, b) $t = 1.5$, c) $t = 2.5$, and d) $t = 3.5$. Building 1 (leftmost) is a "normal" 4-storey building with $k_1 = \ldots = k_4 = 25$, $c_1 = \ldots = c_4 = 10$. Building 2 has the same parameters as building 1 except of $c_1 = \ldots = c_4 = 40$. Building 3 has the same parameters as building 1 but with a smaller value of $k_1 = 2.5$. Building 4 (rightmost) is L-shaped with the same parameters as building 1.

Of course, as we noted, the (deterministic) explicit Euler method is consistent with the $\mathcal{C}^1$ excitation $\ddot{u}$ we expose the ground floor of our building. To take full advantage of higher-order deterministic schemes, on the other hand, a $\mathcal{C}^k$, $k \geq 2$ excitation would be preferable. For $k = 2$ such a ground excitation is gained by applying the Clough-Penzien earthquake model, cf. [7], instead of the Kanai-Tajimi model. Interestingly, when inspecting the final results given in Fig. 9 we see that a smoothing of the initial irregular stochastic impacts occurs through the coupled oscillator equations (i.e., a well known filtering phenomenon). Hence, for any additional oscillator equation or storey of the building the smoothness of the driving excitation for the next storey increases and the potential of higher-order (deterministic) methods begins thus to work in our advantage.

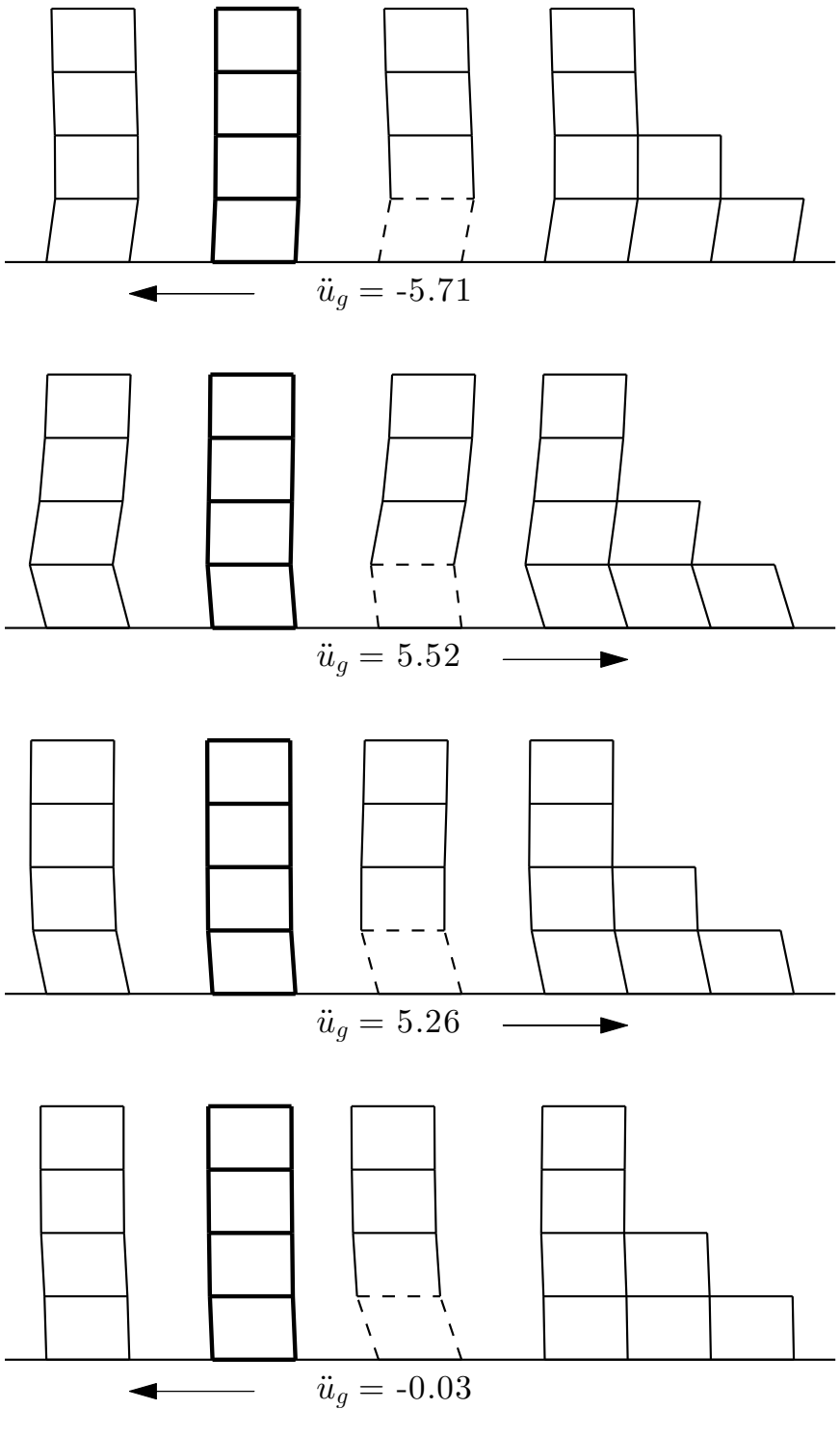

Figure 8: Movement of four different 4-storey buildings under the same stochastic excitation at times a) $t = 0.5$, b) $t = 1.5$, c) $t = 2.5$, and d) $t = 3.5$. (See the text for more details on the characteristics of the buildings.)

III.3 Higher Order Schemes through Implicit Taylor-like Expansions

An alternative approach to obtain explicit schemes of type (III.3) exploits the smoothness of the function f in (II.2) with respect to its variables X_t and ω. The resulting *K-RODE Taylor schemes* were presented by Kloeden and Jentzen in 2007 ([24]; see also [20]), to which the reader is referred for a more detailed discussion.

Let us consider again the initial value problem

$$\frac{\mathrm{d}x}{\mathrm{d}t} = F_\omega(t,x) := f(\omega(t),x), \qquad x(t_0) = x_0, \tag{III.14}$$

for $\omega \in \Omega$.

We wish to carry out the Taylor expansion of the function f with respect to ω and x, for which we consider the *multi-index* $\alpha = (\alpha_1, \alpha_2) \in \mathbb{N}_0^2$. Its magnitude is given by $|\alpha| := \alpha_1 + \alpha_2$, which may take a weight $\gamma \in (0,1]$ such that $|\alpha|_\gamma := \gamma\alpha_1 + \alpha_2$. Likewise, for each $K \in \mathbb{R}_+$ with $K \geq |\alpha|_\gamma$, define $|\alpha|_\lambda^K := K - |\alpha|_\lambda$. Also, let $\alpha! := \alpha_1!\alpha_2!$. Finally, let $f_\alpha := (\partial_1)^{\alpha_1}(\partial_2)^{\alpha_2} f$, with $f_0 = f$.

The k-th order Taylor expansion of f is then given by

$$f(\omega(s),x(s)) = \sum_{|\alpha|\leq k} \frac{f_\alpha(\hat\omega,\hat x)}{\alpha!}(\Delta\omega_s)^{\alpha_1}(\Delta x_s)^{\alpha_2} + R_{k+1}(s), \tag{III.15}$$

with $\Delta\omega_s := \omega(s) - \hat\omega$, where $\hat\omega := \omega(\hat t)$, and $\Delta x_s := x(s) - \hat x$, where $\hat x := x(\hat t)$ for some $\hat t \in [t_0, T)$. The remainder R_{k+1} in (III.15) is then given by

$$R_{k+1}(s) = \sum_{|\alpha|=k+1} \frac{1}{\alpha!} f_\alpha(\hat\omega + \xi_{\omega_s}\Delta\omega_s, \hat x + \xi_{x_s}\Delta x_s)(\Delta\omega_s)^{\alpha_1}(\Delta x_s)^{\alpha_2}, \tag{III.16}$$

for some $\xi_{\omega_s}, \xi_{x_s} \in [0,1]$. The Taylor expansion for f is then inserted into the integral form of the solution of (III.14), namely

$$x(t) = \hat x + \int_{\hat t}^t f(\omega(s),x(s))\mathrm{d}s, \tag{III.17a}$$

$$= \hat x + \sum_{|\alpha|\leq k} \underbrace{\frac{f_\alpha(\hat\omega,\hat x)}{\alpha!}\int_{\hat t}^t (\Delta\omega_s)^{\alpha_1}(\Delta x_s)^{\alpha_2}\mathrm{d}s}_{=:T_\alpha(t;\hat t)} + \int_{\hat t}^t R_{k+1}(s)\mathrm{d}s, \tag{III.17b}$$

$$= \hat x + \sum_{|\alpha|\leq k} T_\alpha(t;\hat t) + \int_{\hat t}^t R_{k+1}(s)\mathrm{d}s. \tag{III.17c}$$

Even though this expansion is implicit in $x(t)$ (which appears after carrying out the integral inside $T_\alpha(t;\hat t)$), one can build up explicit higher order schemes in a recursive manner. This is achieved by approximating the Δx_s terms terms inside T_α using a scheme of one order lower. The way to obtain such schemes is as follows. Let us truncate Eq. (III.17) by ignoring the remainder, and set $t \to \hat t + h$. We have

$$x(\hat t + h) \approx x(\hat t) + \sum_{|\alpha|\leq k} \frac{f_\alpha(\hat\omega,\hat x)}{\alpha!}\int_{\hat t}^{\hat t+h} (\Delta\omega_s)^{\alpha_1}(\Delta x_s)^{\alpha_2}\mathrm{d}s. \tag{III.18}$$

It is now possible to derive the corresponding numerical scheme of order $K \in \mathbb{R}_+$, given by the approximated solution $y_n^{K,h}$, defined for the sets of multi-indices defined by

$$\mathcal{A}_K := \{\alpha = (\alpha_1,\alpha_2) \in \mathbb{N}_0^2 \quad : \quad |\alpha|_\theta = \theta\alpha_1 + \alpha_2 < K\}. \tag{III.19}$$

The $\mathcal{A}_K$-*RODE-Taylor scheme* is then given by

$$y_{n+1}^{K,h} := y_n^{K,h} + \sum_{\mathcal{A}} N_\alpha^{(K)}(t_{n+1}, t_n, y_n^{K,h}), \tag{III.20}$$

where

$$N_\alpha^{(K)}(\hat{t}+h, \hat{t}, \hat{y}) := \frac{1}{\alpha!} f_\alpha(\hat{\omega}, \hat{y}) \int_{\hat{t}}^{\hat{t}+h} (\Delta\omega_s)^{\alpha_1} \left(\Delta y_{\Delta s}^{(|\alpha|_\theta^K)}(\hat{t}, \hat{y}) \right)^{\alpha_2} \mathrm{d}s, \tag{III.21a}$$

$$\Delta y_h^{(\ell)}(\hat{t}, \hat{y}) := \sum_{|\alpha|_\theta < \ell} N_\alpha^{(\ell)}(\hat{t}+h, \hat{t}, \hat{y}), \tag{III.21b}$$

and $\Delta s = s - \hat{t}$. In the notation of Eq. (III.3), this family of schemes has the increment function

$$\phi^{(K)}(h, \hat{t}, \hat{y}) := \frac{1}{h} \sum_{\mathcal{A}} N_\alpha^{(K)}(\hat{t}+h, \hat{t}, \hat{y}). \tag{III.22}$$

Eqs. (III.21a)–(III.21b) reflect the recursivity of the scheme (III.20), since the term $\Delta y_{\Delta s}^{(|\alpha|_\theta^K)}$ is of order $|\alpha|_\theta^K = K - |\alpha|_\theta < K$. The weight θ is taken to be the supremum of the Hölder coefficients of the sample paths derived from the noise process of the RODE [20]. Therefore, two cases should be distinguished:

A) The Hölder continuity holds for the supremum θ;

B) The Hölder continuity does not hold for the supremum θ.

This distinction allows to establish an expression for the local discretisation error of the $\mathcal{A}_K$-RODE-Taylor schemes, defined at the initial step $y_1^{(K,h)}(\hat{t}, \hat{y})$ as

$$L_h^{(K)}(\hat{t}, \hat{y}) := |x(\hat{t}+h, \hat{t}, \hat{y}) - y_1^{(K,h)}(\hat{t}, \hat{y})|. \tag{III.23}$$

Now, define $\tilde{R}_0 := 0$ and, for $K > 0$,

$$\tilde{R}_K := \sup_{0<L\leq K} \max_{\substack{(h,t,x)\in \\ [0,1]\times[t_0,T]\times[-R,R]}} |\phi^{(L)}(h, t, x)|.$$

Finally, let

$$k = k_K := \left\lfloor \frac{K}{\theta} \right\rfloor, \quad R_K := \max\{\tilde{R}_K, \|f\|_{k+1}\}.$$

Under these considerations, the following theorem holds.

Theorem 4. *The local discretisation error for a RODE-Taylor scheme in case A satisfies*

$$\left| L_h^{(K)}(\hat{t}, \hat{x}) \right| \leq C_K h^{K+1}, \tag{III.24}$$

for each $0 \leq h \leq 1$, *where*

$$C_K := (\exp(\|\omega\|_\theta + 2R_K))^{K+1}.$$

In case B, it satisfies

$$\left| L_h^{(K)}(\hat{t}, \hat{x}) \right| \leq C_K^\epsilon h^{K+1-\epsilon}, \tag{III.25}$$

for $\epsilon > 0$ *arbitrarily small, where*

$$C_K^\epsilon := (\exp(\|\omega\|_{\gamma_\epsilon} + 2R_K))^{K+1}, \quad \gamma_\epsilon := \theta - \frac{\epsilon}{(k+1)^2}.$$

Proof. The proof is given in [24]. □

Moreover, the RODE-Taylor schemes converge for each $K > 0$, and the global error behaves as in the ODE case, i.e. it is one order lower than the local error (of order K for case A, and $K - \epsilon$ for case B) [19], [24].

III.4 Numerical Results 2: K-RODE Taylor Schemes

Implementing higher order K-RODE Taylor schemes is a more demanding task, due to its inherent recursiveness. Nevertheless, it turns out that the particular form of Eq. (II.8) simplifies the work, such that, for moderate K, the explicit form of the scheme can be obtained. Take, for instance, $K = 1.0$. The numerical scheme that results from Eq. (III.20) is

$$y_{n+1}^{1.0,h} = y_n^{1.0,h} + hf(O_t, z) + f_{(1,0)}(O_t, z) \int_{t_n}^{t_{n+1}} \Delta O_s \mathrm{d}s,$$

which resembles the Euler method with an additional "correction" term. As a final example, one can verify that, choosing $K = 3.0$ for our right-hand side $f(O_t, z)$, the corresponding RODE Taylor scheme yields

$$\begin{aligned} y_{n+1}^{(3),h} = y_n^{(3),h} + hf + f_{(0,1)} f \frac{h^2}{2} + \frac{h^3}{6} f_{(0,1)}^2 f + f_{(1,0)} \int_{t_n}^{t_{n+1}} \Delta O_s \mathrm{d}s \\ + f_{(0,1)} f_{(1,0)} \int_{t_n}^{t_{n+1}} \int_{t_n}^{s} \Delta O_v \mathrm{d}v \mathrm{d}s + f_{(0,1)}^2 f_{(1,0)} \int_{t_n}^{t_{n+1}} \int_{t_n}^{s} \int_{t_n}^{v} \Delta O_w \mathrm{d}w \mathrm{d}v \mathrm{d}s, \end{aligned} \tag{III.26}$$

where $f_{(0,1)}(O_t, z)$ corresponds to the Jacobian of f, since $z \in \mathbb{R}^2$. Figures 9(a)-(b) show the resulting motion of two independent runs of the normal 4-storey building depicted in Fig. 4(a) using the 3.0-RODE Taylor scheme for the Kanai-Tajimi model with a step size $h = 1/32$. The eight-dimensional equation (II.10) (four positions and four velocities) was solved using a deterministic Runge-Kutta 4 scheme, with all spring constants $k_1 = \ldots = k_4 = 15$ and all damping constants $c_1 = \ldots = c_4 = 5$.

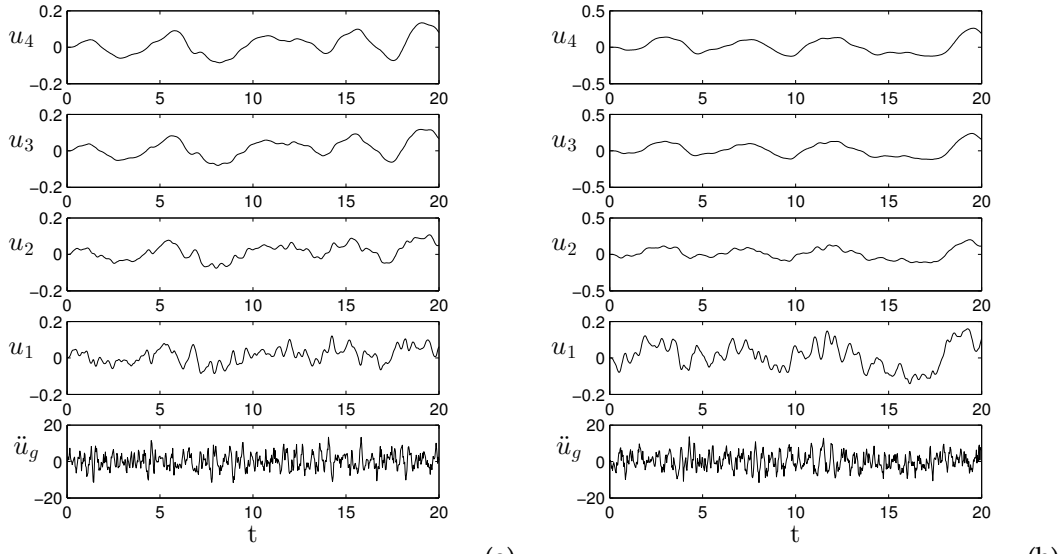

Figure 9: A normal 4-storey building undergoes two different simulations of ground-motion excitation. Depicted are the ground-motion acceleration $\ddot{u}_g$ and the resulting displacement of the four stories of the building as functions of time.

Remark: Numerical Computation of Multiple Integrals in the RODE Taylor Scheme
In (III.26), multiple integrals of the form

$$\int_{t_n}^{t_{n+1}} \int_{t_n}^{s} \Delta O_v \mathrm{d}v\mathrm{d}s \qquad \text{and} \qquad \int_{t_n}^{t_{n+1}} \int_{t_n}^{s} \int_{t_n}^{v} \Delta O_w \mathrm{d}w\mathrm{d}v\mathrm{d}s$$

appear. For the numerical quadrature of these terms, a nested scheme of one-dimensional quadrature rules could be used, but this approach can be overcome by reformulating the multiple integrals as a single one to save computational costs.

For the sake of simplicity, we denote the integrand ΔO_v as $f(v)$ in the following. It is easy to show (see Appendix) that a $(d+1)$-dimensional integration over a one-dimensional function $f(z)$ with particular integration limits relevant in our context can be transformed in the following way:

$$\int_{t_n}^{t_{n+1}} \int_{t_n}^{x_d} \int_{t_n}^{x_{d-1}} \cdots \int_{t_n}^{x_1} f(z)\mathrm{d}z\mathrm{d}x_1 \cdots \mathrm{d}x_d = \int_{t_n}^{t_{n+1}} \frac{1}{d!}(t_{n+1}-z)^d f(z)\mathrm{d}z. \tag{III.27}$$

Numerically, we can approximate Eq. (III.27) with a low-order numerical scheme in the remaining direction. A higher-order quadrature rule is not useful since the integrand involves f, e.g. an Ornstein-Uhlenbeck process, which is only continuous in general. We tested Riemann sums as well as trapezoidal sums. Both numerical integration schemes involve the same amount of computational work and do not differ in the resulting approximation errors. For Riemann sums, the numerical approximation has the following form,

$$\int_{t_n}^{t_{n+1}} \frac{1}{d!}(t_{n+1}-z)^d f(z)\mathrm{d}z \approx \delta \sum_{j=1}^{m} \frac{1}{d!}(t_{n+1}-z_j)^d f(z_j)\ , \tag{III.28}$$

where $z_j := t_n + j\delta$, $\delta = h/m$, and $h = t_{n+1} - t_n$. Therefore, m has to be chosen large enough such that the order of the numerical integral coincides with the order of the K-RODE Taylor scheme.

This way, the multiple integrals are reduced to simple, one-dimensional integrals. This is useful since K-RODE Taylor schemes require the evaluation of multi-dimensional integrals of powers of the stochastic process (e.g. $f(z) = (\Delta O_z)^\beta$).

III.5 Final Remarks on Explicit RODE Methods

The two families of schemes presented so far (averaged schemes and K-RODE Taylor schemes) might appear very different in essence, but their numerical implementation reflects various similarities. Indeed, both require a further subdivision of the chosen timestep h in order to perform the averaging (Eqs.(III.8),(III.10)) or the evaluation of integrals (e.g. Eq. (III.26)), respectively (in the end, such integrals may be interpreted as the mean value of the functions up to a multiplicative constant). The choice of this smaller step size $\delta = h/N$ (resp. h/m) is as crucial to the order of the scheme as the choice of h. In the examples we have presented, in order to achieve an absolute error of order $O(10^{-4})$, one could use an averaged Euler method with $h = 10^{-4}$ and $\delta = 10^{-8}$, or an averaged Heun scheme with $h = 10^{-2}$ and $\delta = 10^{-8}$, or even more, a deterministic (non-averaged) Euler scheme with $h = 10^{-8}$ (since it will be of order $O(h^{1/2})$). Finally, a 3rd order RODE Taylor scheme would require each integral from t_n to t_{n+1} to be calculated with $\delta = h^3 \cdot h$ (order 3 plus performing N such integrals). So, in the end, all four schemes would require the same degree of refinement, namely, 10^{-8}. The authors in [13] clarify that it is the ease of computation of the averages (resp. Riemann sums) as well as the stability of the schemes that makes it preferable to use higher order methods. Likewise, since higher order methods allow us to choose larger h steps, one requires less evaluations of the right hand side vector field f and its derivatives.

Next, we study the key differences between these algorithms for the simulation of random ordinary differential equations and their counterparts for stochastic ordinary differential equations

IV Explicit Numerical Schemes for Stochastic Differential Equations

The numerical theory and simulation of strong solutions of stochastic (ordinary) differential equations is at a very mature level, see [26], [14]. Low order explicit schemes like the Euler-Maruyama or the Milstein method simply belong to the standard tool repertoire of every researcher in the field.

By the order of a numeric scheme we mean, in the context of SDEs, its strong order of convergence as stated in [26], p. 323. Specifically, we say that a discrete time discretization Y^δ with maximum step size δ converges (strongly) to X with order γ at time T if there exists a positive constant C, which does not depend on δ, and a $\delta_0 > 0$ such that

$$\mathbb{E}\left(\left|X_t - Y^\delta(T)\right|\right) \;\leq\; C\delta^\gamma\,,$$

for each $\delta \in (0, \delta_0)$.

IV.1 The Euler-Maruyama & Milstein Schemes for Stochastic Differential Equations

In situations where the paths of the stochastic differential equations are unique in the above mentioned sense, it is illustrative to plot them numerically, as we do throughout this article.

The simplest numerical procedure is the *Euler-Maruyama schema* or *approximation*; the stochastic analogue of Euler's method for deterministic ordinary differential equations.

Consider the one-dimensional stochastic process $X_t = \{X_t : t \in [t_0, T]\}$ satisfying the scalar Itô stochastic differential equation

$$\mathrm{d}X_t \;=\; a(X_t, t)\mathrm{d}t \;+\; b(X_t, t)\mathrm{d}W_t$$

on $t_0 \leq t \leq T$ with the initial condition $X_{t_0} = X_0$. For a given equidistant discretisation[3] $t_0 < t_1 < \cdots < t_n < t_{n+1} < \cdots < t_N = T$ of the time interval $[t_0, T]$, the Euler-Maruyama approximation is a continuous stochastic process $Y_t = \{Y(t) : t \in [t_0, T]\}$ satisfying the iterative scheme

$$Y_{n+1} \;=\; Y_n \;+\; a(Y_n, t_n)\Delta t \;+\; b(Y_n, t_n)\Delta W_t\,, \tag{IV.1}$$

for $n = 0, 1, 2, \ldots, N-1$, where $Y_0 = X_0$,

$$\Delta t \;=\; t_{n+1} \;-\; t_n$$

is the length of the time discretisation subinterval $[t_n, t_{n+1}]$ and

$$\Delta W_t \;=\; W_{t_{n+1}} \;-\; W_{t_n}$$

is the $\mathcal{N}(0, \Delta t)$-distributed increment of the Wiener process on $[t_n, t_{n+1}]$. Y_n is the evaluation of Y_t at the point t_n, i.e., $Y_n = Y(t_n)$.

This one-dimensional procedure can easily be extended to higher dimensions and hence be applied to simulate the solutions of our multi-dimensional problems. Figure 10(a) shows the convergence properties of the Euler-Maruyama scheme applied to Example 1 for $t \in [0, 1]$. As discussed in [26], pp. 341, since the additive diffusive term $b(X_t, t) = (0, 1)^T$ does not depend on X_t, the scheme achieves a strong order of 1.0 (instead of the usual 0.5). The appropriate measure of error is given by

$$\hat{\epsilon} = \frac{1}{N}\sum_{k=1}^{N} |X_{T,k} - Y_{T,k}|,$$

i.e., the mean over N independent runs of the difference of the Euler-Maruyama scheme $Y_{T,k}$ and the exact solution $X_{T,k}$ at time $t = T$. Figure 10(a) was generated with $h = 2^{-1}, \ldots, 2^{-10}$, running $N = 25$ simulations for each time step.

In one dimension, the Euler-Maruyama approximation is easily extended to the *Milstein scheme* by adding the term

$$\tfrac{1}{2} b(x, t) b_x(x, t) \left((\Delta W_t)^2 - \Delta t \right)$$

which results in the iterative scheme

$$\begin{aligned} Y_{n+1} \;&=\; Y_n \;+\; a(Y_n, t_n)\Delta t \;+\; b(Y_n, t_n)\Delta W_t \\ &\quad + \tfrac{1}{2} b(x, t) b_x(x, t) \left((\Delta W_t)^2 - \Delta t \right), \end{aligned}$$

for $n = 0, 1, 2, \ldots, N-1$ and $Y_0 = X_0$. This one-dimensional procedure can easily be extended to higher dimensions and in particular represents a (strong) order one of convergence method for stochastic differential equations.

[3] The choice of an equidistant discretisation leads to a simplification of the notation, but is by no means crucial for the setup of the approximation methods discussed.

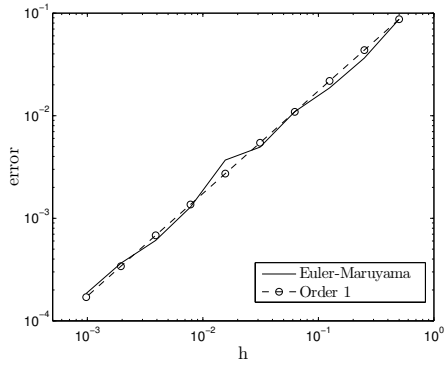

(a)

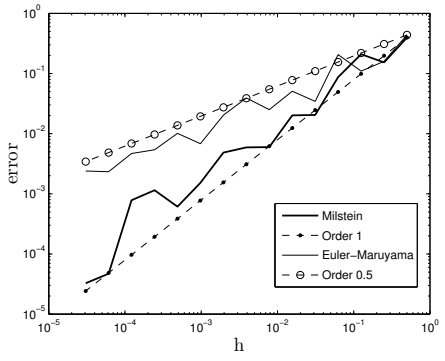

(b)

Figure 10: Application of the Euler-Maruyama method to Example 1 with additive noise (a) and application of the Euler-Maruyama as well as of the Milstein method to the geometric Brownian motion with multiplicative noise (b).

Of course, Example 1 would not be a good test case for the Milstein scheme as, due to the very nature of additive noise, Milstein and the Euler-Maruyama approximation would just be identical. Therefore, Figure 10(b) displays the convergence results of the Milstein-approximation for the famous geometric Brownian motion

$$\mathrm{d}X_t \;=\; aX_t\mathrm{d}t \,+\, bX_t\mathrm{d}W_t\,.$$

and compares them to the convergence of the Euler-Maruyama approximation for the same problem. Recall that the exact solution is given by

$$X_t = X_0 \exp\left(\left(a - \frac{b^2}{2}\right)t + bW_t\right). \tag{IV.2}$$

For the simulation we choose the unstable case $a = 2$ and $b = 1$ where the paths of the geometric Brownian motion tend to infinity instead of converging to zero, with $X_0 = 0.1$. Again, 25 simulations were ran for each $h = 2^{-1}, \ldots, 2^{-15}$.

Finally, Figure 11 shows, in analogy to Figure 9, the application of the Euler-Maruyama approximation to an L-shaped 4-storey building.

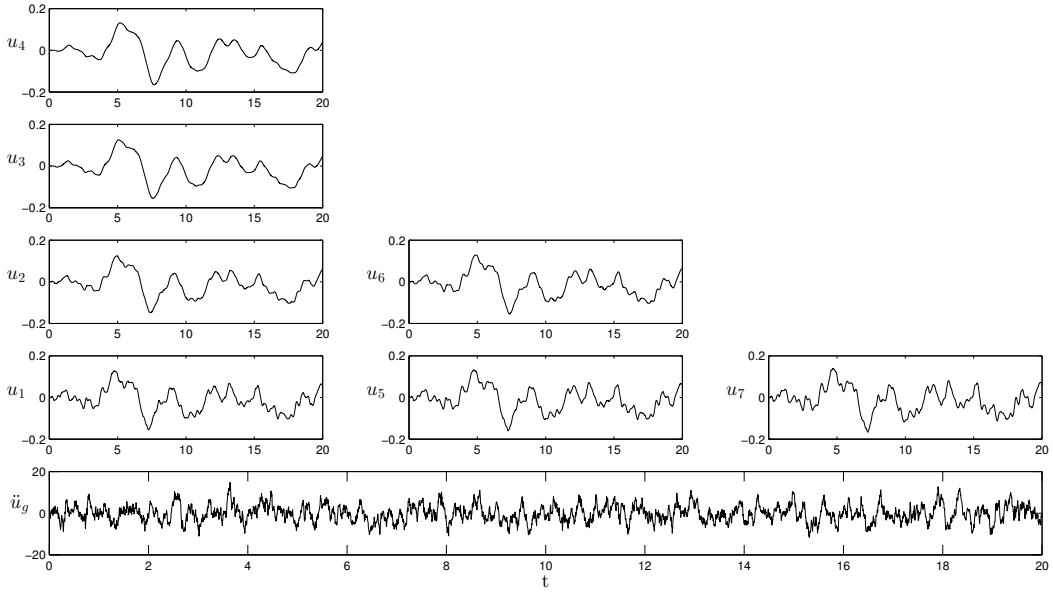

Figure 11: An L-shaped 4-storey building undergoes a simulation of ground-motion excitation calculated with the Euler-Maruyama approximation, using $\Delta t = 0.005$. The ground-motion acceleration $\ddot{u}_g$ and the resulting displacement of the various stories of the building are visualised as functions of time. An additional spring interaction among horizontal neighbours is considered.

IV.2 Multiple Wiener Integrals – Fourier Approach

In general, [26] is acknowledged as the standard reference for SODE numerical schemes. There, higher-order Taylor methods are systematically developed. Apart from the increasing complexity of these schemes, their traditional drawback is the evaluation of multiple Wiener integrals of the type

$$\int_0^t \int_0^{s_3} \int_0^{s_2} f(s_1) \mathrm{d}s_1 \mathrm{d}W_{s_2}^{(2)} \mathrm{d}W_{s_3}^{(1)} \quad \text{or} \quad \int_0^t \int_0^{s_3} \int_0^{s_2} f(s_1) \mathrm{d}W_{s_1}^{(3)} \mathrm{d}W_{s_2}^{(2)} \mathrm{d}W_{s_3}^{(1)} \,,$$

with an appropriate stochastic process f and independent scalar Wiener processes $W_{s_1}^{(3)}$, $W_{s_2}^{(2)}$ and $W_{s_3}^{(1)}$.

Traditionally, the efficient numerical evaluation of such multiple stochastic integrals is challenging as we will see next, cf. [25] and [26], pp. 198, or [11]. Of course, a brute-force approach is always possible though computationally expensive; therefore, a more clever approach is the following one that utilizes the properties of Fourier series representations (cf. [26], pp. 198): Let $W_t^{(i)}$ and $W_t^{(j)}$ with $i \neq j$ be two independent Wiener processes. Then, the starting point for the computation of, say,

$$I(i,j) \;=\; \int_{t_n}^{t_{n+1}} \int_{t_n}^{s_1} \mathrm{d}W_{s_2}^{(i)} \mathrm{d}W_{s_1}^{(j)} \tag{IV.3}$$

is the Brownian bridge process

$$W_t^{(i)} \;-\; \frac{t}{s} W_s^{(i)} \,, \qquad \text{for } 0 \leq t \leq s := \Delta t \,.$$

The Fourier series associated to it reads as

$$W_t^{(i)} \; - \; \frac{t}{s} W_s^{(i)} \;\; = \;\; \tfrac{1}{2} a_{i,0} \; + \; \sum\!\!\!\!\!\!\int k = 1 \left(a_{i,k} \cos\left(\frac{2\pi k t}{s} \right) + b_{i,k} \sin\left(\frac{2\pi k t}{s} \right) \right) ,$$

which is equivalent to

$$W_t^{(i)} \;\; = \;\; \frac{1}{s} W_s^{(i)} t \; + \; \tfrac{1}{2} a_{i,0} \; + \; \sum_{k=1}^{\infty} \left(a_{i,k} \cos\left(\frac{2\pi k t}{s} \right) + b_{i,k} \sin\left(\frac{2\pi k t}{s} \right) \right) , \tag{IV.4}$$

where $a_{i,0} = -2 \sum_{k=0}^{\infty} a_{i,k}$ by setting $t = 0$ and the coefficients $b_{i,j}$ and $a_{i,j}$ are $\mathcal{N}(0, (2\pi^2 k^2) s)$-distributed pairwise independent random variables.

As outlined in [25], this Fourier series can be used to successively derive a hierarchy of multiple stochastic integrals. In particular, it can be shown by first integrating (IV.4) with respect to t over $[0, s]$ and then with respect to $W_t^{(j)}$ over $[0, s]$, that the following relation is true:

$$I(i,j) \;\; = \;\; \tfrac{1}{2} W_s^{(i)} W_s^{(j)} \; - \; \tfrac{1}{2} \left(a_{j,0} W_s^{(i)} - a_{i,0} W_s^{(j)} \right) \; + \; s A_{i,j} \, ,$$

where

$$A_{i,j} \;\; = \;\; \tfrac{\pi}{s} \sum_{k=1}^{\infty} k \left(a_{i,k} b_{j,k} - a_{j,k} b_{i,k} \right) .$$

A truncation method is required in order to computationally handle these infinite series. One observes first, that

$$\xi_i \;\; := \;\; \tfrac{1}{\sqrt{s}} W_s^{(i)} \, , \qquad \xi_{i,k} \;\; := \;\; \sqrt{\tfrac{2}{s}} \pi k a_{i,k} \, , \qquad \eta_{i,k} \;\; := \;\; \sqrt{\tfrac{2}{s}} \pi k b_{i,k}$$

are independent normally distributed random variables that can be conveniently sampled prior to computation. Let $p \in \mathbb{N}$ denote a truncation index such that $I(i,j) \approx I(i,j)^p$, where the approximation $I(i,j)^p$ of $I(i,j)$ is given as

$$I(i,j)^p \;\; = \;\; \tfrac{1}{2} s \xi_i \xi_j \; - \; \tfrac{\sqrt{s}}{2} \left(a_{j,0}^p \xi_i - a_{i,0}^p \xi_j \right) \; + \; s A_{i,j}^p \, ,$$

with

$$A_{i,j}^p \;\; = \;\; \tfrac{1}{2\pi} \sum_{k=1}^{p} \tfrac{1}{k} \left(\xi_{i,k} \eta_{j,k} - \xi_{j,k} \eta_{i,k} \right) \quad \text{and} \quad a_{i,0}^p \;\; = \;\; - \frac{\sqrt{2s}}{\pi} \sum_{k=1}^{p} \tfrac{1}{k} \xi_{i,k} \, .$$

The mean-square error of this approximation is discussed in [25], and in order to achieve, for instance, a strong order of convergence one for the Milstein scheme with this approximation of the multiple stochastic integrals [11] suggests that p should be chosen of order $\mathcal{O}(s^{-1})$. A method to reduce the number p is proposed in [36].

A very efficient and pragmatic alternative to the extremely cumbersome Fourier series ansatz for the simulation of multiple stochastic integrals in a higher-order scheme is to apply a lower-order method, like the Euler-Mayurama scheme, on each sub-interval with a very fine step size, cf. [23].

IV.3 Multiple Wiener Integrals – Multi-dimensional Approach

Following our considerations on multiple Ornstein-Uhlenbeck integrals (see Remark at the end of Sec. III.4 and Appendix), multiple Wiener integrals of the form (IV.3) can also be formulated as higher-dimensional integrals. The major difference is now the independence of the individual

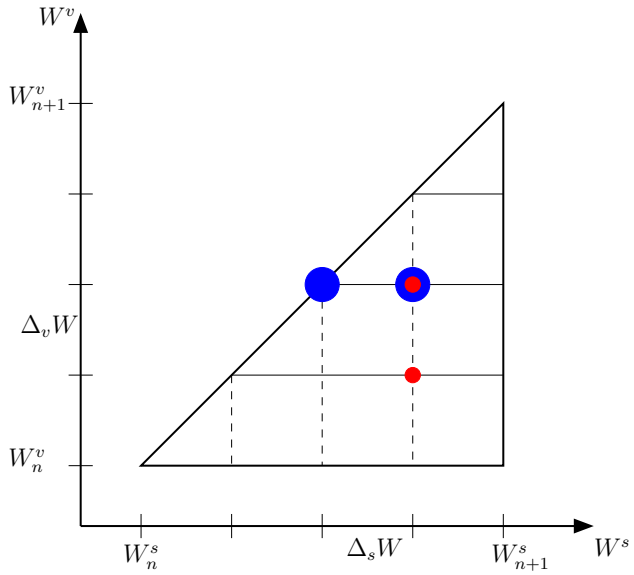

Figure 12: Interpreting the double integration in time over v and s ($v, s \in [t_n, t_{n+1}]$) as a 2D spatial integration on a triangular domain. Along one axis direction, the orthogonal W always has constant values (e.g., constant W^v but different W^s for the two blue vertices).

Wiener processes which does not allow for the analytical reduction of the multiplicity of integrals into a polynomial factor in the integrand any more. In Fig. 12, this fact is visualised for two Wiener processes $W^{(s)}$ and $W^{(v)}$: For integrating an overall coarse time step $\Delta t_n := t_{n+1} - t_n$, the two red locations contain identical values of $W^{(s)}$ in the integrand but different values of $W^{(v)}$, whereas the blue locations differ in values for $W^{(s)}$ with identical values of $W^{(v)}$.

However, rewriting multiple Wiener integrals as multi-dimensional ones motivates another approach: Applying quadrature rules in the higher-dimensional space as approximations and reformulating those in a computationally efficient manner. Consider a discretisation of the multiple Wiener integrals for the example (IV.3) of the form

$$I(i,j) = \int_{t_n}^{t_{n+1}} \int_{t_n}^{s_1} f(v_2) \mathrm{d}W_{v_2}^{(i)} \mathrm{d}W_{v_1}^{(j)} \tag{IV.5}$$

$$\approx \sum_{j=1}^{M_j} \left(\sum_{i=1}^{M_i} f(v_i) \underbrace{\left(W_{v_{i+1}}^{(i)} - W_{v_i}^{(i)} \right)}_{=:\Delta_i W} \right) \underbrace{\left(W_{v_{j+1}}^{(j)} - W_{v_{j+1}}^{(j)} \right)}_{=:\Delta_j W}, \tag{IV.6}$$

where M_i and M_j represent the number of subintervals used for the discretisation of the two axis i, j of the two different processes, respectively. For the sake of simplicity in the notation, we assume identical subintervals ($M_i \equiv M_j =: M$) in the following. The mesh sizes for the midpoint

rule are denoted by $\Delta_i W$ and $\Delta_j W$, respectively. We rewrite the sums in (IV.6) as

$$\begin{aligned} I(i,j) &\approx \sum_{j=1}^{M} \Delta_j W \cdot [f(v_1)\cdot\Delta_{i=1}W + f(v_2)\cdot\Delta_{i=2}W + \ldots + f(v_M)\cdot\Delta_{i=M}W] \\ &= \underbrace{f(v_1)\cdot\Delta_{i=1}W}_{=:A_1}\cdot\Delta_{j=1}W + \underbrace{(f(v_1)\cdot\Delta_{i=1}W + f(v_2)\cdot\Delta_{i=2}W)}_{=:A_2}\cdot\Delta_{j=2}W \\ &\quad + \underbrace{(f(v_1)\cdot\Delta_{i=1}W + f(v_2)\cdot\Delta_{i=2}W + f(v_3)\cdot\Delta_{i=3}W)}_{=:A_3}\cdot\Delta_{j=3}W + \ldots \end{aligned} \tag{IV.7}$$

The key observation now is that the mesh sizes as factors of the summands in (IV.7) are constant on axis-aligned straight lines in one of the two directions i and j, respectively (cf. Fig. 12). Hence, a single computation of those mesh sizes is sufficient for the multi-dimensional integration; combined with storing the intermediate sums in a variable throughout the calculations[4], we only need a single, one-dimensional loop of length M in order to compute the whole two-dimensional quadrature rule on the triangle-shaped domain.

The mulit-dimensional approach directly translates to higher-order scenarios (in the sense of higher multiplicity of the integrals) with analogue formulas.

The multi-dimensional approach has, from our point of view, three nice features. First, its direct relation to classical quadrature schemes provides means to choose suitable mesh sizes (i.e. suitable values for M) directly compared to a bit more cryptic representation of p in the usual approach. Second, It is very straightforward to implement. Third, the computational costs—while being in the same order of complexity—are lower since only additions and multiplications have to be performed (no fractions or square roots etc.). For a huge number of evaluations such as in a long-term or high-accuracy time integration (where a large number of coarse time steps $\Delta t := t_{n+1} - t_n$ have to be calculated), these low costs may represent a non-negligible advantage.

V Résumé

Effective and efficient numerical methods for stochastic and random (ordinary) differential equations play an important role in the sciences, in engineering and computational finance.

Here, from an applied point of view the key features of the rather new methods for RODEs are discussed with a focus on the averaged Euler and Heun as well as an implicit 3.0-RODE Taylor method. Details for their successful implementation in multi-dimensional applications were presented together with an outline of their advantages and drawbacks are given. Wherever possible we compared them with the corresponding schemes for SODEs to highlight the links between the underlying two types of noise driven differential equations.

Beyond this survey-like character, we studied the application of these RODE and SODE methods on one- and multi-dimensional examples, in particular, the problem of ground-motion-induced excitation of multi-storey buildings subject to the Kanai-Tajimi earthquake model. Moreover, we discuss an efficient ansatz for the evaluation of multiple Ornstein-Uhlenbeck integrals as they occur in higher-order RODE schemas and extend it to the efficient evaluation of multiple Wiener integrals that are common in higher-order SODE methods.

[4]This variable will simply add A_i in the ith loop iteration to its former value.

References

[1] H.W. Alt (1999): *Lineare Funktionalanalysis*, 3rd ed., Springer-Verlag.

[2] A.E. Bashirov (2003): *Partially Observable Linear Systems under Dependent Noises*, Birkäuser Verlag.

[3] D. Brigo and F. Mercurio (2006): *Interest Rate Models – Theory and Practice with Smile, Inflation and Credit*, 2nd ed., Springer-Verlag.

[4] H. Bunke (1972): *Gewöhnliche Differentialgleichungen mit Zufälligen Parametern*, Akademie Verlag.

[5] A.K. Chopra (2006): *Dynamics of Structures: Theory and Applications in Earthquake Engineering*, 3rd edition, Prentice Hall Publishing.

[6] K.L. Chung (2002): *Green, Brown, and Probability & Brownian Motion on the Line*, World Scientific Publishers.

[7] R. W. Clough and J. Penzien (1975): *Dynamics of Structures*, McGraw-Hill, New York.

[8] H. Doss (1977): *Liens Entre Equations Differentielles Stochastiques et Ordinaires*, Annales de l'Institut Henri Poincare (B), 13(2), pp. 99-125.

[9] A. Friedman (2006): *Stochastic Differential Equations and Applications*, Dover Publications.

[10] D.T. Gillespie (1996): *Exact Numerical Simulation of the Ornstein-Uhlenbeck Process and Its Integral*, Physical Review E, 54(2), pp. 2084-2091.

[11] H. Gilsing and T. Shardlow (2007): *SDELab: A Package for Solving Stochastic Differential Equations in MATLAB*, J. Comp. Appl. Math., 205, pp. 1002-1018.

[12] G.H. Golub and J.M. Ortega (1992): *Scientific Computing and Differential Equations*, Academic Press.

[13] L. Grüne and P.E. Kloeden (2001): *Pathwise Approximation of Random Ordinary Differential Equations*, BIT Numerical Mathematics, 41(4), pp. 711-721.

[14] D.J. Higham (2001): *An Algorithmic Introduction to Numerical Simulation of Stochastic Differential Equations*, SIAM Review, 43(3), pp. 525-546.

[15] G.W. Housner and P.C. Jenning (1964): *Generation of Artificial Earthquakes*, Journal of the Engineering Mechanical Division, ASCE, 90, pp. 113-150.

[16] P. Imkeller and B. Schmalfuss (2001): *The Conjugacy of Stochastic and Random Differential Equations and the Existence of Global Attractors*, Journal of Dynamics and Differential Equations, 13(2), pp. 215-249.

[17] P. Imkeller and Ch. Lederer (2002): *The Cohomology of Stochastic and Random Differential Equations, and Local Lineraization of Stochastic Flows*, Stochastics and Dynamics, 2(2), pp. 131-159.

[18] R. N. Iyengar and C. S. Manohar (1987): *Nonstationary Random Critical Seismic Excitations*, Journal of Engineering Mechanics, 113(4), pp. 529-541.

[19] A. Jentzen (2007): *Numerische Verfahren Hoher Ordnung für Zufällige Differentialgleichungen*, Diplomarbeit, J.W. Goethe Universität, Frankfurt am Main.

[20] A. Jentzen and P.E. Kloeden (2011): *Taylor Approximations for Stochastic Partial Differential Equations*, CBMS-NSF Regional Conference Series in Applied Mathematics (No. 83), SIAM Press.

[21] K. Kanai (1957): *Semi-Empirical Formula for the Characteristics of the Ground*, Bulletin of the Earthquake Research Institute, 35.

[22] K. Kanai (1961): *An Empirical Formula for the Spectrum of Strong Earthquake Motions*, Bulletin of the Earthquake Research Institute, 39.

[23] P.E. Kloeden (2002): *The Systematic Derivation of Higher Order Numerical Methods for Stochastic Differential Equations*, Milan J. Math., 70, pp. 187-207.

[24] P.E. Kloeden and A. Jentzen (2007): *Pathwise Convergent Higher Order Numerical Schemes for Random Ordinary Differential Equations*, Proc. R. Soc. A, 463, pp. 2929-2944.

[25] P.E. Kloeden, E. Platen and I.W. Wright (1992): *The Approximation of Multiple Stochastic Integrals*, Stoch. Anal. Appl., 10, pp. 431-441.

[26] P.E. Kloeden and E. Platen (1999): *Numerical Solution of Stochastic Differential Equations*, 3rd corrected ed., Springer-Verlag.

[27] J.H. Lawton (1988): *More Time Means More Variation*, Nature, p. 563.

[28] Y.K. Lin and G.Q. Cai (2004): *Probabilistic Structural Dynamics*, McGraw-Hill Publishing.

[29] T. Neckel and F. Rupp (1992): *Random Differential Equations in Scientific Computing – Motivation, Theory & Simulation*, Versita/ De Gruyter Publishing.

[30] L.G. Paparizos (1986): *Some Observations on the Random Response of Hysteretic Systems*, Earthquake Engineering Research Laboratory, Report No. EERL 86-02, Pasadena, California.

[31] P.E. Protter (2005): *Stochastic Integration and Differential Equations*, 2nd ed., Springer-Verlag.

[32] S. Rezaeian and A. der Kiureghian (2010): *Stochastic Modeling and Simulation of Ground Motions for Performance-Based Earthquake Engineering*, PEER Report 2010/02 Pacific Earthquake Engineering Research Center, College of Engineering, University of California, Berkely.

[33] H.J. Sussmann (1978): *On the Gap Between Deterministic and Stochastic Differential Equations*, Annals of Probability, 6(1), pp. 19-41.

[34] H. Tajimi (1960): *A Statistical Method of Determining the Maximum Response of a Building During an Earthquake*, Proceedings of the Second World Conference on Earthquake Engineering, Tokyo and Kyoto, Japan, Vol. II.

[35] Y.K. Wen (1995): *Inelastic Structures under Nonstationary Random Excitation*, pp. 411-435, In W. Kliemann and N. S. Namachchivaya (Eds.): Nonlinear Dynamics and Stochastic Mechanics, CRC Mathematical Modelling Series.

[36] M. Wiktorsson (2001): *Joint Characteristic Function and Simultaneous Simulation of Iterated Ito Integrals for Multiple Independent Brownian Motions*, Ann. Appl. Probab., 11, pp. 470-487.

Appendix: Higher-dimensional integrals of one dimensional functions

Using induction, it is easy to show that the following holds:

$$\int_{t_n}^{t_{n+1}} \int_{t_n}^{x_d} \int_{t_n}^{x_{d-1}} \cdots \int_{t_n}^{x_1} f(z)\mathrm{d}z\mathrm{d}x_1 \cdots \mathrm{d}x_d = \int_{t_n}^{t_{n+1}} \frac{1}{d!}(t_{n+1}-z)^d f(z)\mathrm{d}z \,. \tag{V.1}$$

This formula is also known as the Cauchy formula for repeated integration.

Proof. The base case is formulated for $d = 1$, where changing the order of the integration allows to formulate the double integral as a single one,

$$\int_{t_n}^{t_{n+1}} \int_{t_n}^{s} f(v)\mathrm{d}v\mathrm{d}s = \int_{t_n}^{t_{n+1}} \int_{v}^{t_{n+1}} f(v)\mathrm{d}s\mathrm{d}v = \int_{t_n}^{t_{n+1}} (t_{n+1}-v)f(v)\mathrm{d}v, \tag{V.2}$$

since the integrand f does not depend on s.

To see that it holds for dimension $d+1$, we use the induction assumption (V.1), evaluate it at $t_{n+1} = x_{d+1}$, and integrate both sides from t_n to t_{n+1} w.r.t. x_{d+1}. Hence,

$$\begin{aligned}
\int_{t_n}^{t_{n+1}} \int_{t_n}^{x_{d+1}} \int_{t_n}^{x_d} \cdots \int_{t_n}^{x_1} f(z)\mathrm{d}z\mathrm{d}x_1 \cdots \mathrm{d}x_d\mathrm{d}x_{d+1} = \\
\int_{t_n}^{t_{n+1}} \int_{t_n}^{x_{d+1}} \frac{1}{d!}(x_{d+1}-z)^d f(z)\mathrm{d}z\mathrm{d}x_{d+1} = \\
\int_{t_n}^{t_{n+1}} \int_{z}^{t_{n+1}} \frac{1}{d!}(x_{d+1}-z)^d f(z)\mathrm{d}x_{d+1}\mathrm{d}z = \\
\int_{t_n}^{t_{n+1}} \left[\frac{1}{(d+1)!}(x_{d+1}-z)^{(d+1)} f(z)\right]_{z}^{t_{n+1}} \mathrm{d}z = \\
\int_{t_n}^{t_{n+1}} \frac{1}{(d+1)!}(t_{n+1}-z)^{(d+1)} f(z)\mathrm{d}z \,,
\end{aligned} \tag{V.3}$$

which shows the assertion. □

Note that the base case $d = 1$ as well as the case $d = 2$ can also be visualised by interpreting the multiple integrals over the same axis (time) as a multiple integral in space on a restricted domain.

In the case of the double integral for $d = 1$, the idea is quite obvious. Interpreting the two integration variables v and s as axes in a 2D grid, one needs to integrate constant functions over the domain as depicted in Fig. 13.

For the triple integral ($d = 2$), the same idea applies. Interpreting the triple integral in time as a 3D spatial integral with dimensions s, v, and w, we have to restrict the integration domain to a simplex (see Fig. 14). We integrate the cross sections on the (s, v)-planes first (i.e. getting areas of triangles) and then integrate over w:

$$\int_{t_n}^{t_{n+1}} \int_{t_n}^{s} \int_{t_n}^{v} f(w)\mathrm{d}w\mathrm{d}v\mathrm{d}s = \int_{t_n}^{t_{n+1}} \frac{1}{2}(t_{n+1}-w)^2 f(w)\mathrm{d}w \,.$$

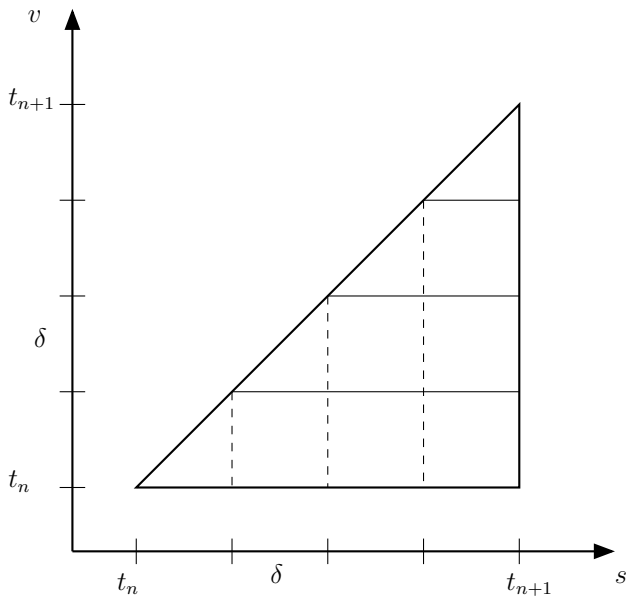

Figure 13: Interpreting the double integration in time over v and s as a 2D spatial integration on a triangular domain: The function $f(v)$ is constant w.r.t. s and is integrated over a domain (interval) which decreases linearly with v.

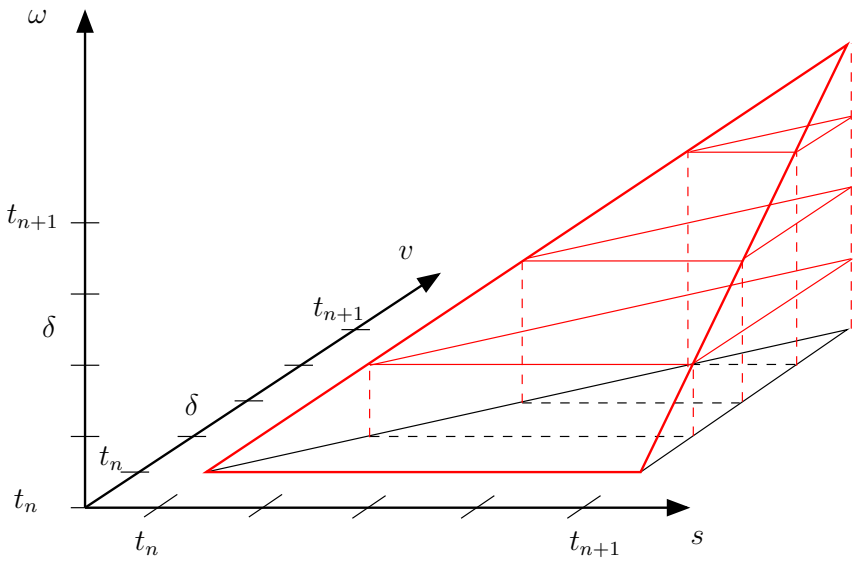

Figure 14: Interpreting the triple integration in time as a 3D spatial integration on a simplex domain: Triangle areas have to be computed which depend decreasingly linearly on the innermost variable w.